NUREG/CR-4924
LA-11013-MS

Seismic Category I Structures Program Final Report, FY 1983-84

Los Alamos National Laboratory
Los Alamos, New Mexico 87545

NUREG/CR-4924
LA-11013-MS

RA

Seismic Category I Structures Program Final Report, FY 1983-84

Richard C. Dove*
Joel G. Bennett
Charles Farrar
Charles A. Anderson

Manuscript submitted: April 1987
Date published: September 1987

Prepared for
Division of Engineering
Office of Nuclear Regulatory Research
US Nuclear Regulatory Commission
Washington, DC 20555

NRC FIN No. A7221

*Consultant at Los Alamos. 0764 C.R. 65, Del Norte, CO 81132.

Los Alamos National Laboratory
Los Alamos, New Mexico 87545

CONTENTS

FIGURES

TABLES

SEISMIC CATEGORY I STRUCTURES PROGRAM
FINAL REPORT, FY 1983-84

by

Richard C. Dove, Joel G. Bennett, Charles Farrar, Charles A. Anderson

ABSTRACT

This report summarizes the results obtained from a series of simulated seismic tests on scale models of a prototypical Category I nuclear power plant auxilliary building, representing a reinforced concrete, diesel generator building. Two sizes of model structures were used: 1/10 scale and 1/30 scale. Model construction, test methods, instrumentation, data reduction techniques, experimental results, comparison of experimental and computed results, and conclusions are presented in this report. Values of structural stiffness obtained from both static and dynamic tests are found to be significantly lower than values of stiffness computed using the usual design methods. Values of modal frequency obtained from dynamic tests are compared to computed values. Decreasing modal frequencies with increasing seismic input are reported. The effective damping of these test structures is determined from the test results. The results obtained from the two different size (1/10- and 1/30-scale) models are compared.

I. INTRODUCTION

The Seismic Category I Structures Program currently being carried out at the Los Alamos National Laboratory (LANL) is sponsored by the Engineering Branch, Division of Engineering Safety, of the Nuclear Regulatory Commission (NRC). This project is part of a program designed to increase confidence in

the assessment of Category I nuclear power plant structural behavior beyond the design limit. The project is focused on answering questions regarding safety issues that may arise when existing nuclear facilities are subjected to higher seismic loads than those considered in their original design. The program involves the design, construction, and testing of reinforced concrete models of auxiliary buildings, fuel-handling buildings, etc., but does not include the reactor containment building. The overall goal of the program is to supply to the Nuclear Regulatory Commission experimental information and a validated procedure to establish the sensitivity of the dynamic response of these structures to earthquakes of magnitude beyond the design basis earthquake. The main purposes of the experimental program are (1) to obtain general information about the way in which these structures behave in the inelastic range as compared with their behavior in the elastic range, (2) to provide stiffness and damping values for more demanding loadings on the structures, (3) to identify for use in design of systems and components changes in floor response spectra as the structures are loaded into the inelastic range, and (4) to provide experimental data for benchmarking inelastic structural analysis codes.

More information on the background of this program is found in Ref. 1. During FY 82, preliminary experiments were conducted on small, reinforced-concrete isolated shear walls (see Fig. 1), identified as the most important element in the Category I structures of interest in this program.

This preliminary experimental program was intended to serve the following purposes:

1. Perfect the construction techniques necessary to fabricate the small reinforced-concrete structures.
2. Design and evaluate the test equipment and instrumentation necessary to conduct appropriate static and dynamic tests.
3. Conduct and analyze the results of a sufficient number of tests to determine the relative merits of static tests, conventional vibration tests, and simulated seismic tests.

These preliminary experiments, completed in FY 82, are reported in detail in Ref. 2. The most significant results of these tests, conducted on 1/30-scale models (where the prototype wall thickness is assumed to be 30 in.), are summarized below.

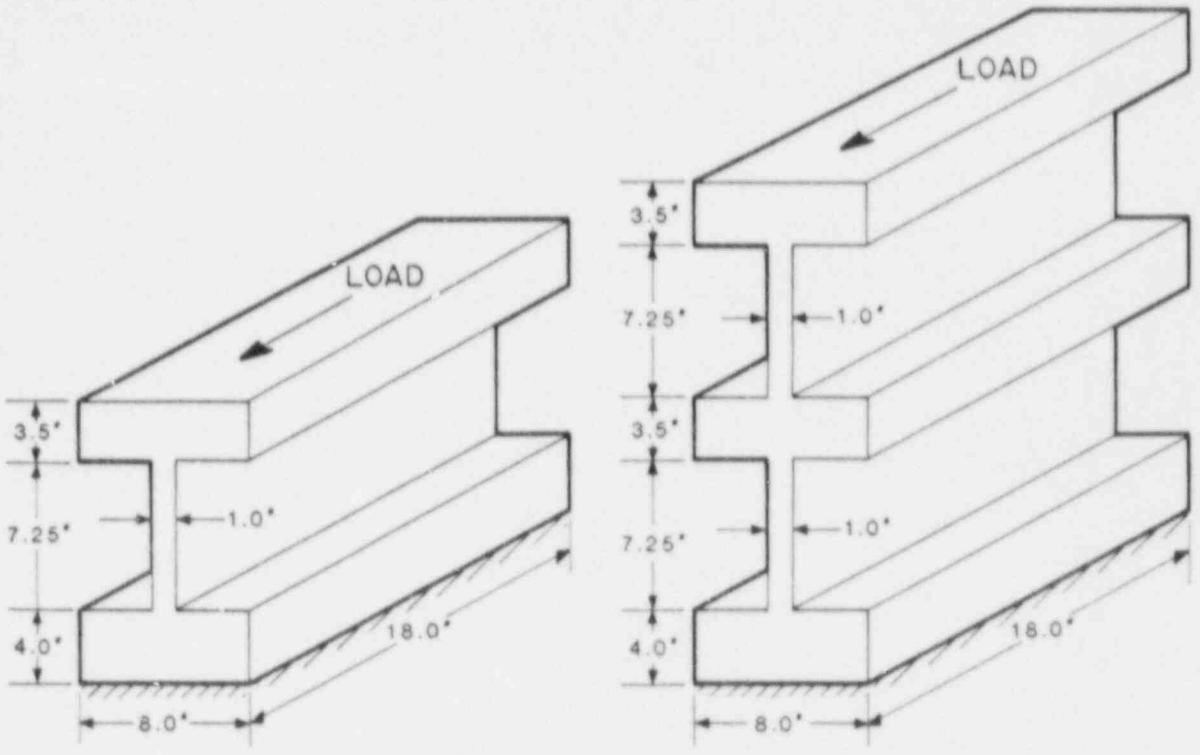

Fig. 1. Isolated shear wall structures.

1. At high-load levels (7 g on the model wall or 0.6 g on a prototype wall), reinforced-concrete shear walls behave in a highly nonlinear and inelastic manner.
2. The load levels at which these walls crack and fail are in reasonable agreement with the values computed using the standard design methods as specified in ACI 349. However, the stiffness of these walls is found to be considerably less than the value of stiffness calculated by the usual design methods.
3. During load cycling, such as would occur during a seismic event, reinforced-concrete shear walls exhibit significant hysteretic energy loss. The amount of energy loss per cycle, and hence the effective damping, is dependent upon load level (about 7 g on the models, 0.6 g on a prototype wall).
4. At higher load levels, the measured acceleration response is considerably less than would be predicted by a linear response spectrum. This latter finding is in agreement with the result predicted by the

Newmark-Hall Nonlinear Design Response Spectrum.[3] To our knowledge, this is the only experimental verification of this nonlinear approach for the analysis of shear wall-type structures.

5. Standard vibrating test methods (such as sine sweeps and resonance search and dwell) that are widely used to evaluate damping ratios, modal frequencies, and mode shapes for many structures and machines, were found to be both inadequate and inappropriate when applied to reinforced-concrete shear walls, even at moderate load levels. The reason is that the properties of stiffness and damping of the reinforced-concrete shear walls change continually with load cycling, and the load cycle history associated with these conventional vibration tests is in no way representative of the load cycle history associated with seismic responses. As a result of this finding, all of the subsequent dynamic tests carried out as a part of this program used simulated seismic loading. It is important to note, however, that two of the most widely quoted studies of high-load tests on reinforced-concrete structures used sinusoidal vibration excitation.[4,5]

The transition of the testing of isolated shear walls to small-scale structures began in FY 83. The structures were models of a prototypical Category I, two-story, diesel generator building. The shape and dimensions of the assumed prototype structure are shown in Fig. 2, together with the dimension of two scaled versions of this structure.* The 1/30- and 1/10-scale models were tested during FY 83 and 84 and the results of these tests are presented in this report. Although preliminary static and dynamic tests were conducted on the one-story, 1/30-scale models, the emphasis was on simulated seismic tests of two-story structures during which the models were driven by an appropriately scaled version of the 1940 El Centro N-S earthquake accelerogram.

II. CONSTRUCTION OF MODEL STRUCTURES

All of the structures tested during FY 83 and 84 were small-scale models of a prototypical Category I, diesel generator building. The shape and

*Figure 2 shows a two-story structure; however, several single-story versions of the 1/30-scale structure were also constructed and tested.

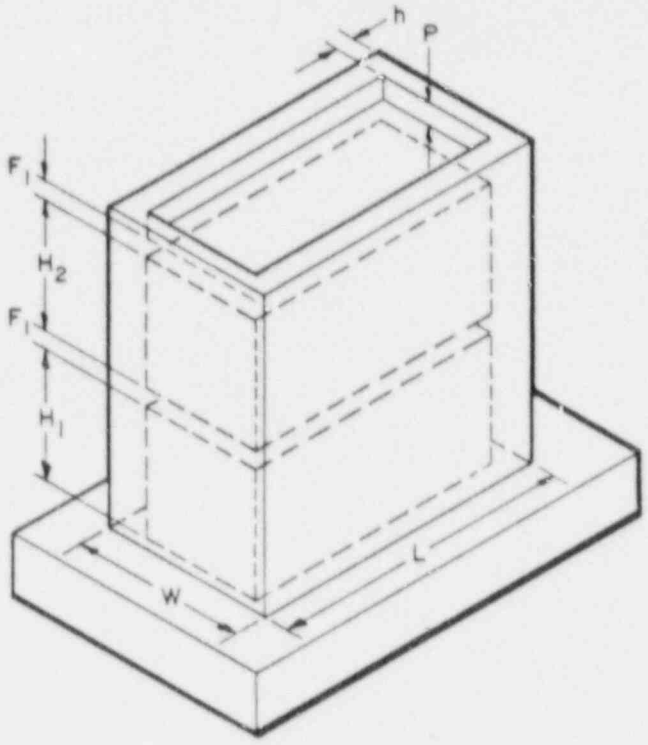

	h, F_1, F_2	W	L	H_1 & H_2	P	Wt/STORY*(lb)
1/30 SCALE	1 in.	10 in.	18 in.	7.25 in.	1 in.	47.7
1/10 SCALE	3 in.	30 in.	54 in.	21.75 in.	3 in.	1286
PROTOTYPE	30 in.	25 ft	45 ft	18 ft, 1.5 in.	30 in.	1,286,000

*BASE NOT INCLUDED

Fig. 2. Two-story structure: model and prototype.

dimensions of the assumed prototype structure are shown in Fig. 2, together with the dimensions of the two scaled versions of this structure.

The model structures were constructed using a microconcrete having the properties given in Table I.

In the 1/30-scale models, the reinforcement consisted of 1/2-in. welded, (nonwoven), square mesh hardware cloth at each wall surface. This resulted in 0.28% reinforcement in each direction, on both wall surfaces. The 1/10-scale models were reinforced using a deformed model reinforcing rod obtained from the Portland Cement Association (PCA designation D-1-1). This rod was tied in a 1.0-in. square mesh and placed at each wall surface to give the same percentage reinforcement as was used in the 1/30-scale model.

TABLE I

CONCRETE PROPERTIES

Property	1/30-Scale Models (1-in. thick wall)	1/10-Scale Models (3-in. thick wall)
Ultimate compressive strength, f'_c	2040 - 3270 psi	3180 - 3330 psi
Tensile strength, f_t	270 - 440 psi	375 - 430 psi
Modulus of elasticity, E	2.3-2.6 x 10^6 psi	2.8 x 10^6 psi

The nominal reinforcement material properties are shown in Table II.

All of the model structures that were constructed and tested during this program are listed in Table I-A in Appendix A. The material properties obtained from compression and split cylinder tests conducted on test cylinders cast during the construction of each model structure and concrete modulus and reinforcement material properties are given in Table II-A in Appendix A.

Regardless of scale, the sequence of model construction was the same. The base slab was cast with reinforcing wires or bars embedded in the slab at the wall locations,* and the base slab concrete was roughened where the walls would join the base. After the base slab had hardened, the reinforcing and forms for the first-story walls and ceiling were put in place. Next the microconcrete was placed and tamped and/or tamped and vibrated. The second-story construction was similar to the first story. After casting, the 1/30-scale models

TABLE II

REINFORCING PROPERTIES

Property	1/30-Scale Models (1-in. thick wall)	1/10-Scale Models (3-in. thick wall)
Wire diameter	0.042 in.	0.113 in.
Yield stress	42,700 psi	42,400 psi
Ultimate tensile strength	53,100 psi	50,000 psi
Modulus of elasticity	25.6 x 10^6 psi	28.5 x 10^6 psi
Elongation	4 per cent	13.1 per cent

*In one series of tests the effect of embeddment depth was investigated.

were placed into a moist chamber for 2 weeks of curing. The 1/10-scale models were wrapped in plastic during the curing period, because they were too large for the moist chamber.

Figure 3 shows a single-story, 1/30-scale structure during construction; the base mat has been cast, the reinforcement has been assembled, and the inside and outside forms (plexiglass) are in place. Figure 4 shows a 1/10-scale structure during construction. The base and first story have been cast and forms (marine plywood) stripped, and the second-story reinforcement and inside forms are in place.

III. EXPERIMENTAL PROGRAM

A. Preliminary Static Tests: Single-Story, 1/30-Scale Structures

Eleven, single-story, 1/30-scale models of the diesel generator building were statically tested to failure under both monotonic and cyclic load conditions. The purpose of these tests was to compare measured values of stiffness, cracking load, and ultimate load with the values obtained by calculation using material properties and geometry.

The tests we conducted used the same horizontal axis, 20,000-lb force, servohydraulic testing machine that had been used in the isolated shear wall

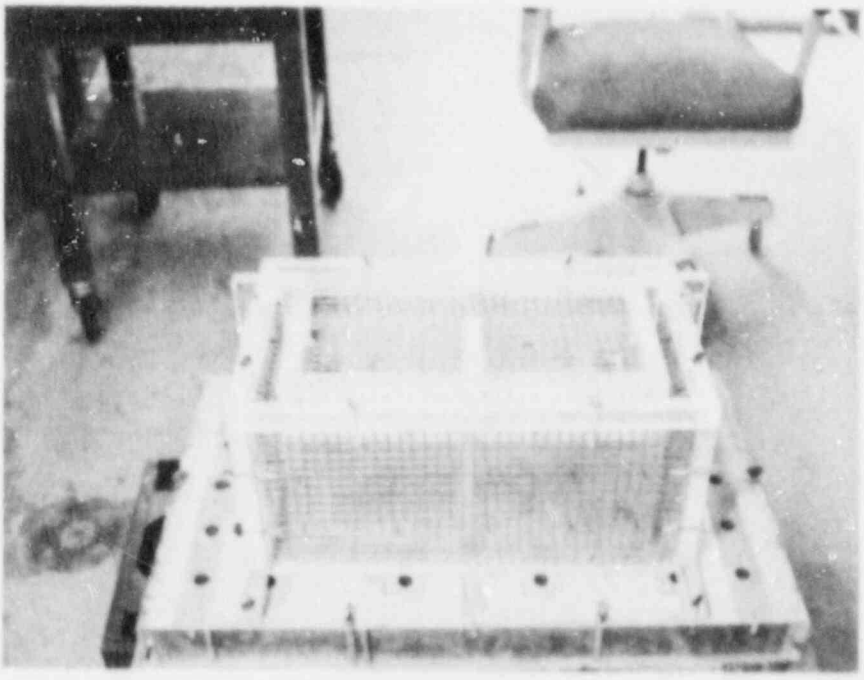

Fig. 3. A single-story, 1/30-scale structure under construction.

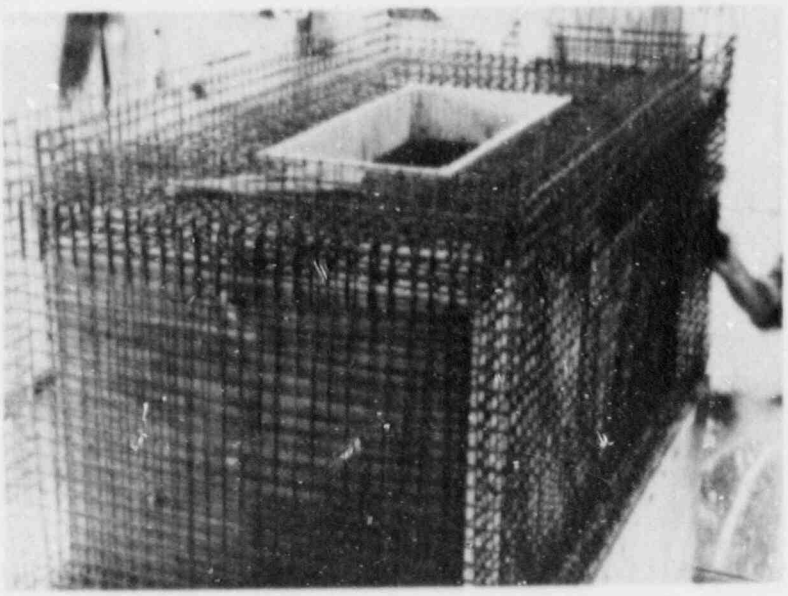

Fig. 4. A two-story, 1/10-scale structure under construction.

tests. See Ref. 2 for more details. Models were tested with the load applied either parallel to the longer dimension (longitudinal load) or parallel to the shorter dimension (transverse load). The load was applied through a 1-in.-thick steel plate that was rigidly clamped around the entire perimeter at the top of the walls. A rigid frame, clamped to the upper surface of the structure's base, supported displacement transducers that measured the horizontal movement of the roof slab and base slab. The data recorded are plotted as load vs relative deformation diagrams, that is, roof slab motion minus base slab motion. Figure 5 shows a structure in the test machine; the holding frame and the displacement transducers on one end (a similar set is mounted on the far end) are visible. In this photo, the loading plate has not yet been bolted to the top of the structure. In Fig. 6 the top plate has been bolted to the structure and connected to the hydraulic ram (at the far end), and the structure is ready for a longitudinal load test.

The two structures subjected to cyclic loading (No. 3D-8 in the transverse direction and No. 3D-9 in the longitudinal direction) behaved in much the same way as the isolated shear walls that had been tested using cyclic loading (see Ref. 2). That is, below a threshold value the hysteresis loop in the load vs deformation diagram is small and does not grow as the load is cycled at a fixed

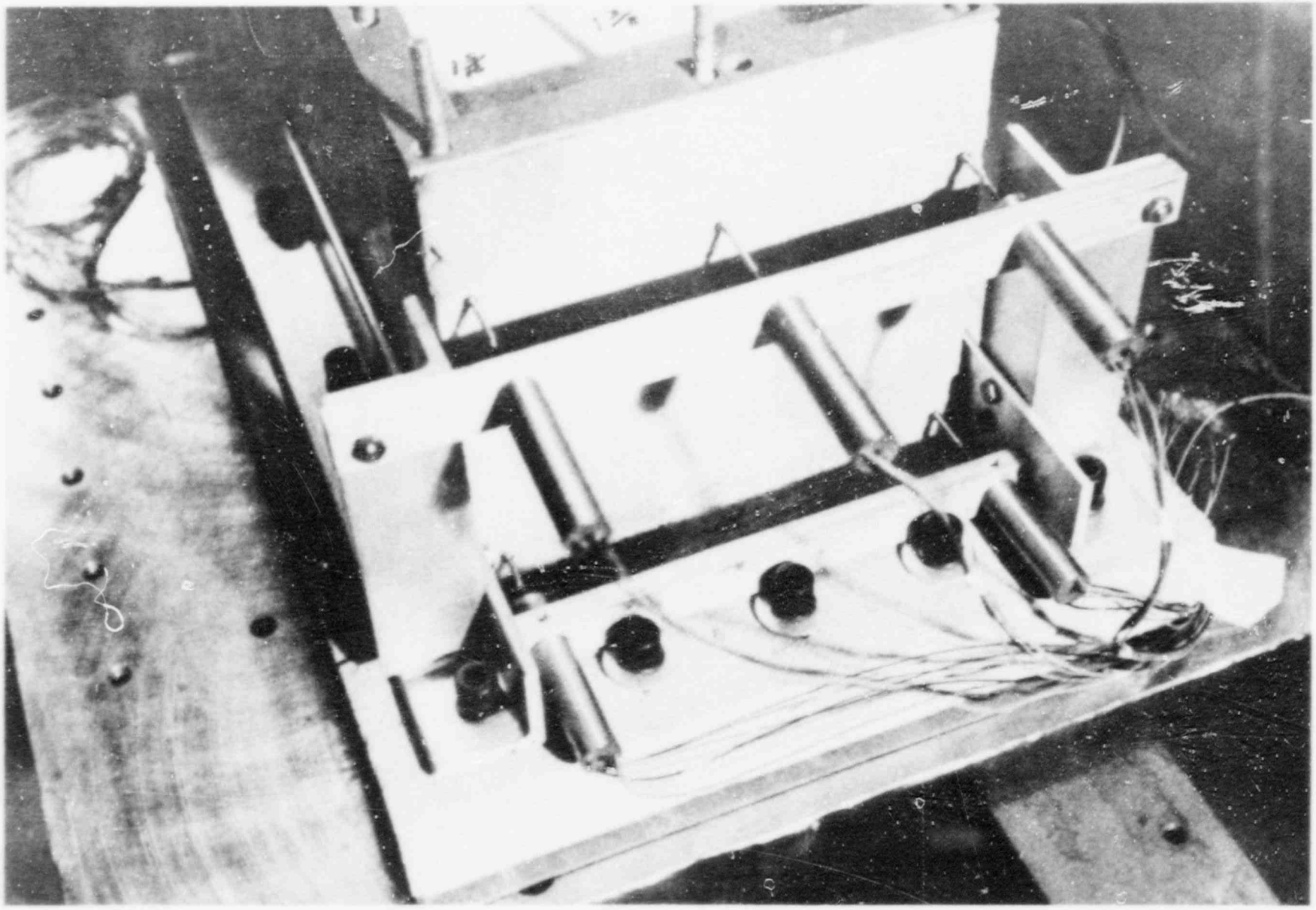

Fig. 5. Displacement measurement: 1/30-scale, static test setup.

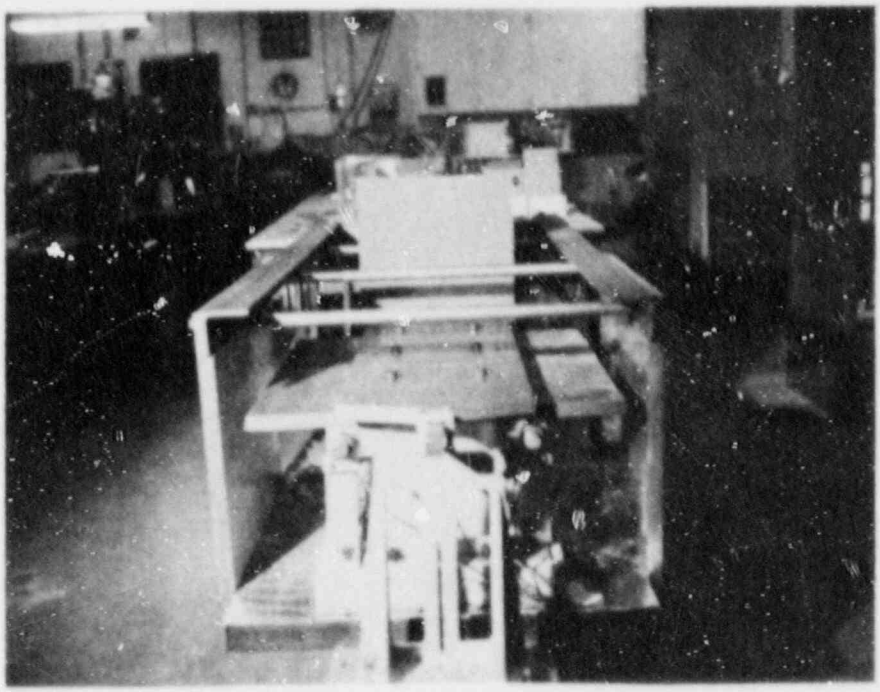

Fig. 6. Static, longitudinal load test: 1/30-scale structure.

level. Above this threshold value, the area inside the hysteresis loops increase with both increase in load level and load cycling at a fixed load level.

The structures subjected to monotonic loading also behaved in much the same way as the isolated shear walls that had been tested previously under monotonic loading. Figures 7 and 8 show two structures that were failed by monotonic loading. Structure No. 3D-4, shown in Fig. 7, was loaded in the longitudinal direction. Notice that, although 45° cracks due to shear have developed, there is also some "lifting" from the base slab that may have increased the ultimate deformation and decreased the ultimate load. However, this partial base failure should have had no effect on the measured low-load property evaluation. Structure 3D-2, shown in Fig. 8, was loaded in the transverse direction. The 45° cracks, due to shear, were well-developed before the long wall collapsed.

Figures 9 and 10 show the force vs deformation diagrams obtained from these two monotonic tests. The small steps visible in these curves, marked C_1, C_2, etc., are associated with crack formation. As was the case with the

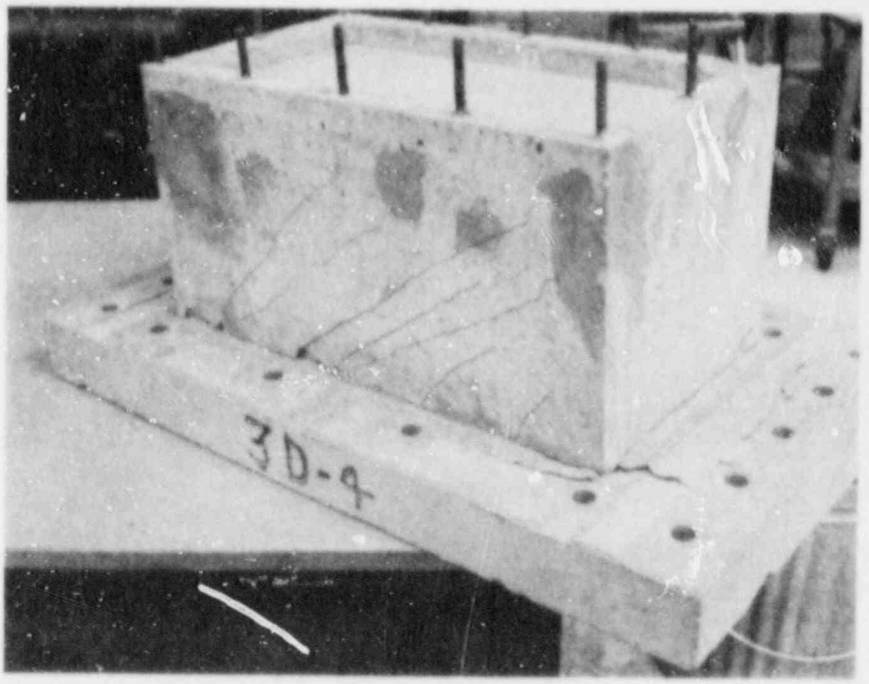

Fig. 7. Single-story, 1/30-scale structure failed by monotonic, longitudinal static load.

isolated shear walls, there is no truly linear region in these load vs deformation diagrams; therefore, the way in which the structural stiffness (K) is defined and, hence, evaluated is of great importance.

The tangent modulus at the origin will, of course, give the largest value for the stiffness (K); however, this value does not appear to be the desired value K used to compute the expected modal frequencies and response motions when the structure is seismically loaded to a relatively high level. For predicting response in the large-load region, it might be argued that K should be evaluated as the secant modulus at the load level necessary to produce cracking (P_c). This has been done for structure 3D-2 in Fig. 10, and, as shown, gives a value of K (at $P = P_c$) = 0.54×10^6 lb/in.

Since the modulus of elasticity (E) of normal weight concrete is often evaluated as the secant modulus of the stress vs strain curve at a stress level of 50% of the ultimate stress (see ASTM C469), it may be reasonable and consistent to evaluate the structural stiffness (K) as the secant modulus of the load vs deflection curve at a load level of 50% of the ultimate load. This also has been done for structure 3D-2 on Fig. 10, and, as shown, gives a

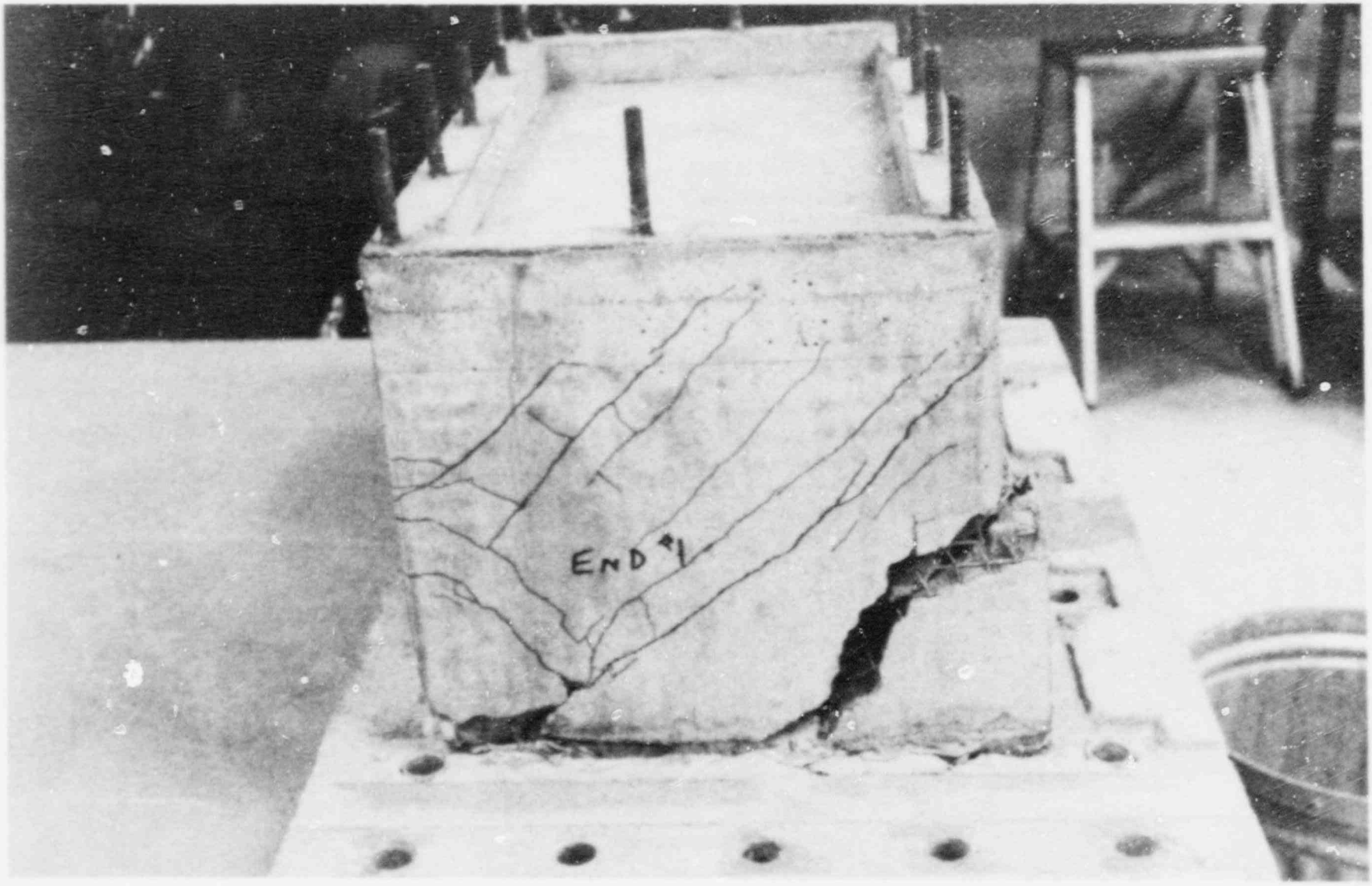

Fig. 8. Single-story, 1/30-scale structure failed by monotonic, transverse static load.

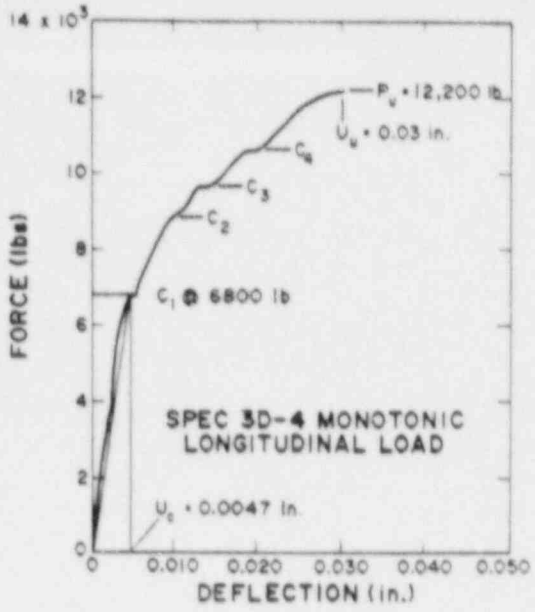

Fig. 9. Load vs deflection: monotonic, longitudinal test.

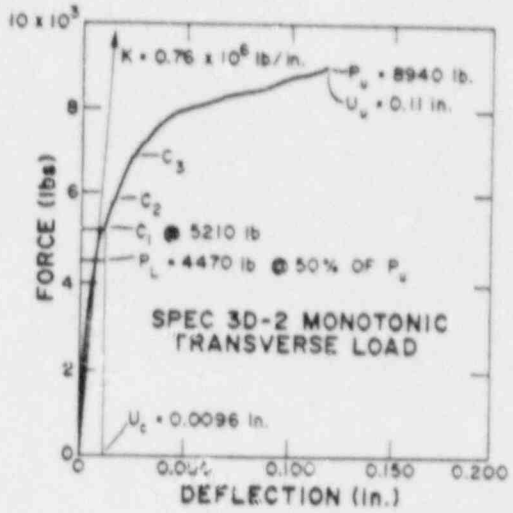

Fig. 10. Load vs deflection: monotonic, transverse test.

value of K (at $P_L = P_U/2$) = 0.76×10^6 lb/in. This latter method (K evaluated at $P_L = P_U/2$) has been used to evaluate the stiffness of all of the 1/30-scale, single-story structures that were statically tested. The results from these tests on 11 structures are given in Table III.

Notice that only two structures (3D-4 and 3D-9) were tested with loading in the longitudinal direction. This was the result of the decision to conduct all simulated seismic tests with loading in the transverse direction. Also note that only two structures (3D-8 and 3D-9) were subjected to cyclic loading. This was the result of the observation that load cycling had little effect on the property value of greatest interest (K, evaluated at 50% of ultimate load).

Some of these structures (3D-7, 10, 11, 12, 13, 19, and 20) were deliberately aged for different times (from less than 1 hr, tested immediately after removal from the 100% humidity chamber, to 48 weeks) in an attempt to investigate the effect of aging on the structural properties. Inspection of Table III and Fig. 11 shows that there is no apparent correlation between age and either stiffness (K) or ultimate load (P_U). These same structures also were given different amounts of reinforcement embedment depth in the base slab (see Fig. 11) to determine the effect of this variable on failure mode. No effect was noted.

TABLE III

RESULTS FROM STATIC TESTS

(1/30-Scale, Single-Story Structures)

Structure (Number)Age(Weeks)	Load* Type	f'_c** (psi)	Ultimate Load P_u(lb)	Modulus*** E(psi x 10^6)	Stiffness K (lb/in. x 10^6) Measured†	Computed††	Ratio
3D - 2/(9)	M,T	2700	8940	2.96	0.76	2.90	3.82
3D - 8/(7)	C,T	2300	6100	2.73	0.80	2.63	3.35
3D - 7/(48)	M,T	2350	5880	2.76	0.92	2.71	2.95
3D - 10/(24)	M,T	3270	4900	3.26	1.14	3.19	2.80
3D - 11/(6)	M,T	3090	7100	3.17	0.92	3.11	3.38
3D - 12/(12)	M,T	2050	6330	2.58	1.23	2.53	2.06
3D - 13/(3)	M,T	2040	4500	2.57	0.88	2.52	2.86
3D - 19/(0)	M,T	N.A.	5980	N.A.	0.87	N.A.	N.A.
3D - 20/(0)	M,T	N.A.	5600	N.A.	1.02	N.A.	N.A.
3D - 4/(5)	M,L	3320	12200	3.28	1.74	6.08	3.49
3D - 9/(8)	C,L	2690	9100	2.96	1.67	5.47	3.28

* M - monotonic; C - cyclic; T - transverse; L - longitudinal.

** Average of tests results from five, 1-in. diam. x 2-in.-long cylinders.

*** $E = 57{,}000\sqrt{f'_c}$. See Ref. 6.

† K evaluated as the secant modulus of the load vs deflection plot at a load level of $P_u/2$, where P_u is the maximum load.

†† Computed using $E = 57{,}000\sqrt{f'_c}$, see text (Discussion of Results) for details of this computation.

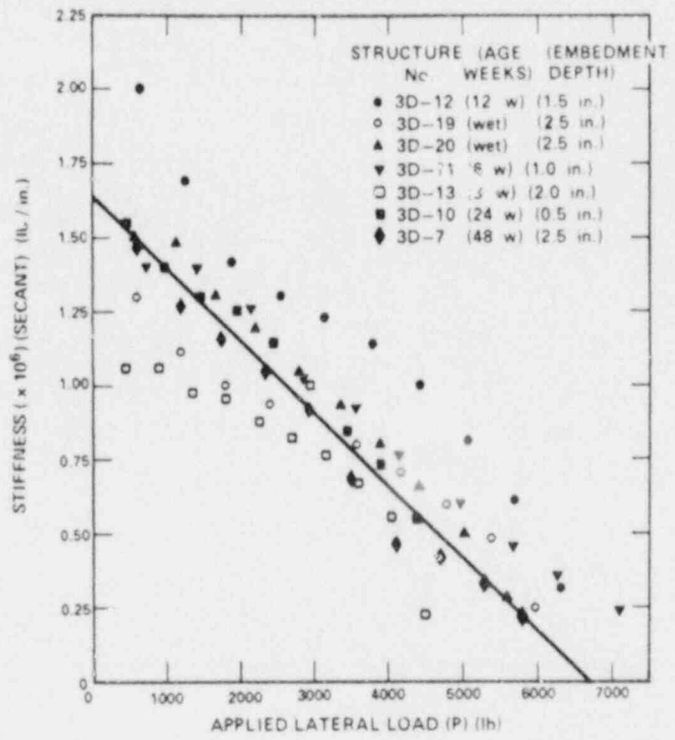

Fig. 11. Effect of aging on stiffness modulus.

The values of structural stiffness (K) that were determined from these static tests were compared to the values calculated from material properties and geometry using the usual mechanics-of-materials methods. These calculations are shown and the comparison is discussed in the Discussion of Results.

B. Preliminary Dynamic Tests; Single-Story, 1/30-Scale Structures

Two single-story, 1/30-scale structures were subjected to 0.5-g broad-band random base excitation to measure their effective elastic region resonant or modal frequency (f). This value (f) is used to calculate a "dynamic" stiffness that can be compared to either the stiffness calculated from material properties or to the stiffness as measured in static tests. These tests were conducted on the 20,000-lb (force) electrodynamic shaker previously used to test the isolated shear walls at the Los Alamos National Laboratory (see Ref. 2).

Figure 12 shows a structure mounted on the shake table ready for transverse direction testing. Numerous accelerometers and displacement transducers were monitored during these tests, but the essential data taken were the following:

$\ddot{Y}$ (t) - the acceleration-time history of the input (base) motion.

$\ddot{X}$ (t) - the acceleration-time history of the response motion at the roof level.

The modal frequency was measured in the following manner. The structure was subjected to a 0.25-g - 0.5-g base acceleration ($\ddot{Y}$).* Both the input signal Y(t) and the response signal $\ddot{X}(t)$ were recorded, and the transfer function T.F.[$\ddot{X}(t)/\ddot{Y}(t)$] was computed. The modal frequency was obtained from the transfer function presented in the phase and amplitude plots as shown in Fig. 13.

To compute the effective stiffness (K) from this dynamic test data, it is necessary to measure the modal frequency, as explained in the previous paragraph, using the same structure, but with different amounts of mass added to the structure. Structure 3D-5 was tested at low acceleration (02.5-0.5 g) levels under three conditions: (1) no mass added to the structure, (2) approximately 130 lb added, and (3) approximately 230 lb added. Mass was added by clamping steel plates to the top of the structure. Figure 12 shows the structure with 231 lb of weight added. Structure 3D-6 was tested with no mass added and with 230 lb added.

Using the measured modal frequencies from two tests in which different amount of mass (M_A) were added to the structure, it is possible to eliminate the effective distributed mass of the structure (M_O) from the relationship between modal frequency (ω), total mass (M_T), and effective stiffness (K), thus

$$K = \omega_O^2 M_O = \omega_T^2 (M_O + M_{ADDED}) ,$$

or

$$M_O = M_{ADDED}/[(\omega_O/\omega_T)^2 - 1] ,$$

*The excitation level is low to minimize damage due to testing, because the low-load level stiffness is the property desired from this test. The signal may be either broad-band random or a scaled version of the 1940 El Centro N-S that was used in later tests. The minimum input acceleration level for good signal reproducibility was used and generally was about 0.25-0.5 g for these models.

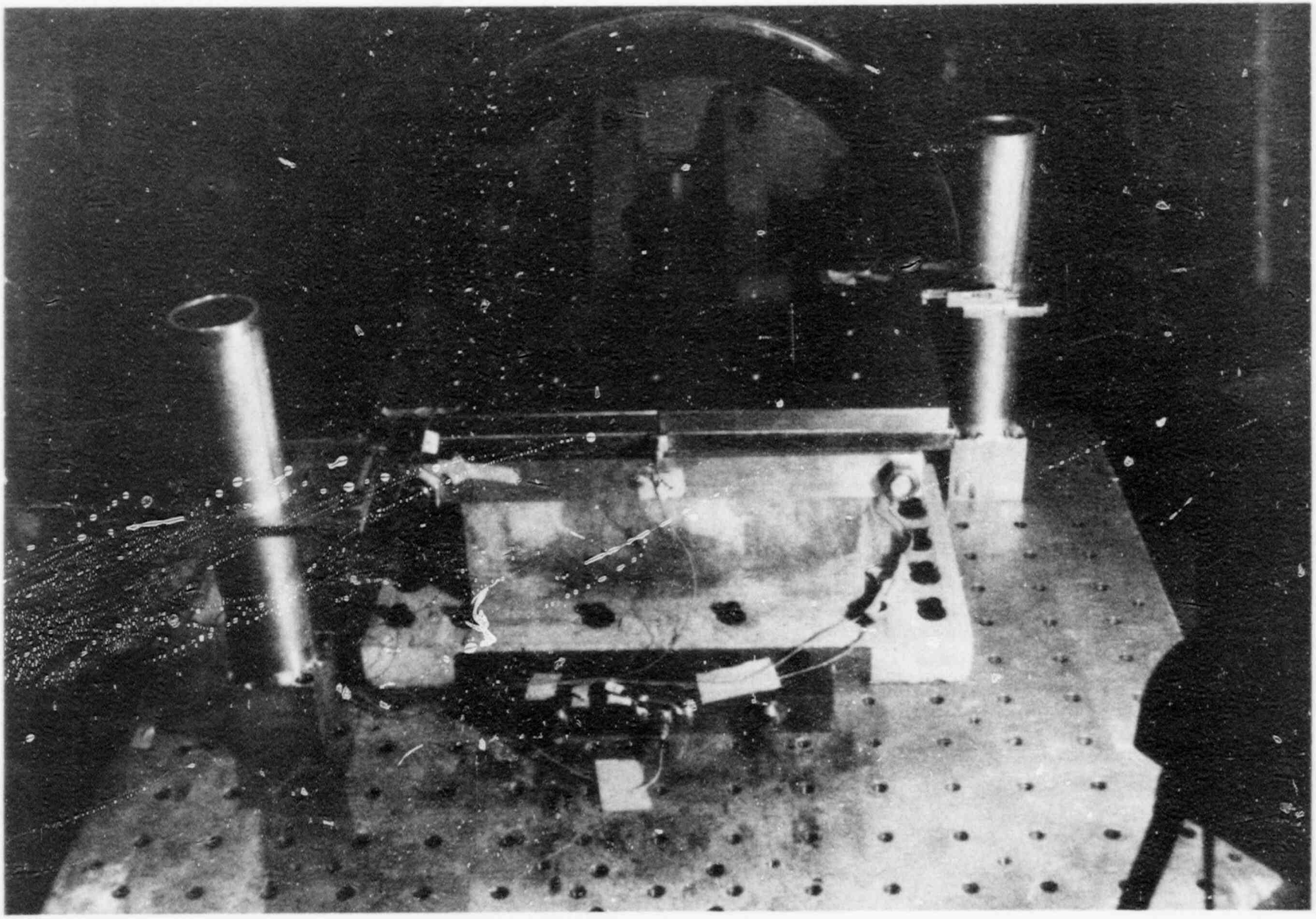

Fig. 12. Single-story, 1/30-scale structure mounted on shake table.

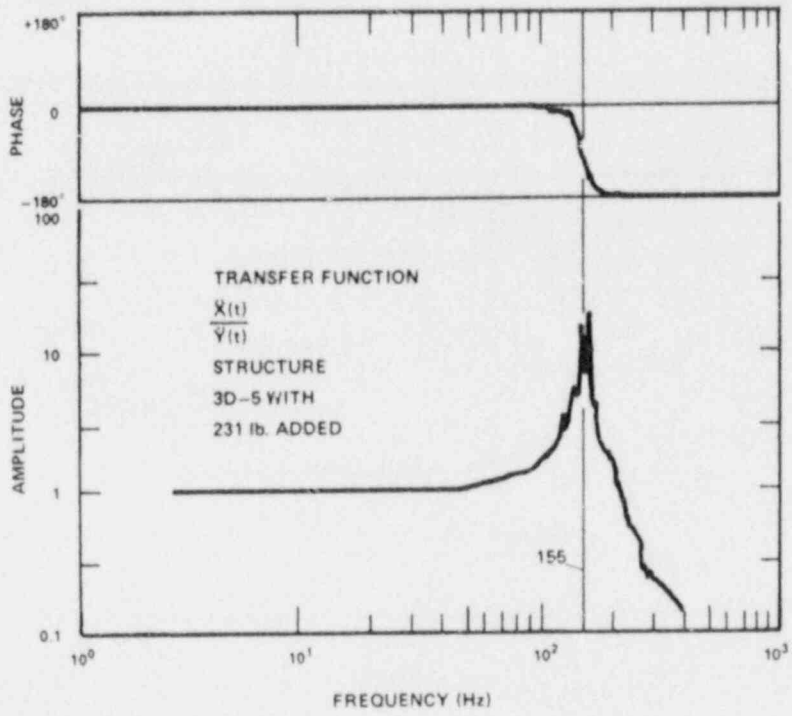

Fig. 13. Sample transfer function plot.

in which

ω_o = the measured modal frequency with no added mass,

ω_T = the measured modal frequency with a given amount of mass added, and

M_{ADDED} = the amount of mass added.

By substituting the second equation back into the first, we can compute the structure's stiffness (K) from the data without the necessity of deciding upon the lumped mass equivalent of the structure's distributed mass.* The stiffnesses obtained using the above method on the two single-story, 1/30-scale models are given in Table IV.

*It is also possible to determine the effective distributed mass (M_o) from this data. For structure 3D-5, M_o is found to be 19.2 lbs, which is in good agreement with the values obtained by taking the top slab mass (10.7 lb) plus the mass of wall for a height equal to twice the slab thickness (2 x 4.36 = 8.72 lb).

TABLE IV

RESULTS FROM DYNAMIC TESTS

(1/30-Scale, Single-Story Structures)

Structure (No.)	Load* (Type)	f'_c** (psi)	$57000\sqrt{f'_c}$*** (psi x 10^5)	Measured† Modal Freq. (Hz)	Stiffness (K lb/in. x 10^6) (Cal)	(Test)	Ratio K_{Cal}/K_{Test}	Remarks
3D-5	M,T	2620	2.91	212	2.86	0.69	4.14	3rd test, 130 lb added
	M,T	2620	2.91	155	2.86	0.62	4.61	4th test 230 lb added
	M,L	2620	2.91	325	5.40	1.54	3.51	1st test, 130 lb added
	M,L	2620	2.91	247	5.40	1.51	3.58	2nd test, 230 lb added
3D-6	M,T	2500	2.85	167	2.79	0.71	3.93	1st test, 230 lb added

* M - monotonic; C - cyclic; T - transverse; L - longitudinal.

** Average of tests results from five, 1-in. diam. x 2-in.-long cylinders.

*** $E = 57{,}000\sqrt{f'_c}$; see Ref. 6.

† 3D-5 first-mode freq. with no added mass was 950 Hz longitudinal and 560 Hz transverse.
3D-6 first-mode freq. with no added mass was 560 Hz transverse.

These results are compared to stiffness values obtained by calculation and from the static tests in the section titled "Discussion of Results." These measured modal frequencies were also useful in designing and interpreting the results of the simulated seismic tests that were conducted on 1/30- and 1/10-scale two-story structures. These simulated seismic tests, which were the main thrust of this program, are described in the following section.

C. Simulated Seismic Tests: Two-Story, 1/30- and 1/10-Scale Structures

These tests were conducted to develop information about the following parameters:

1. values of effective stiffness (K) and damping (ζ), and the way in which these values vary with earthquake magnitude, as measured by peak acceleration ($\ddot{Y}_{pk}$),
2. peak acceleration input required to produce nonlinear/inelastic response,
3. peak acceleration input required to produce failure of the structure, and
4. the way in which floor response spectra are affected by the level of input acceleration.

Furthermore, since results were obtained from two sizes of structures (1/30 scale and 1/10 scale), they can be compared, thus providing a partial check of the scaling. Finally, the results obtained can be projected to predict prototype behavior by utilizing the appropriate scaling laws.

Three, two-story, 1/30-scale structures were fabricated and tested on the LANL electrodynamic shake table (Fig. 14). Two 1/10-scale, two-story structures were built at Los Alamos and transported to the Construction Engineering Research Laboratory (CERL) located at Champaign, Illinois. Figure 15 shows a 1/10-scale structure mounted on the servohydraulically driven table at CERL. The specification of the two test facilities are given in Appendix B.

Except during some preliminary tests at 0.25 g levels, lumped masses (steel plates) were added to these structures so that the 1/30-scale structure was a true 1/3-scale model of the 1/10-scale structure. Also, except during these low-acceleration-level preliminary tests, the excitation signal was a properly scaled version of the 1940 El Centro N-S accelerogram. The scaling of the models and the test signal are discussed in detail in Appendix C.

During these tests, numerous accelerometers and displacement transducers were mounted on the structure. Figure 16 illustrates a typical instrumentation

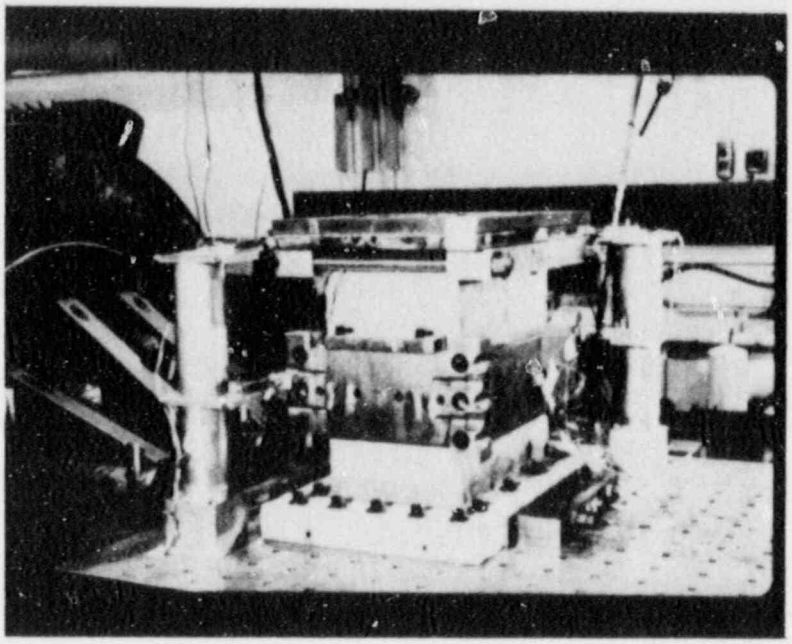

Fig. 14. A two-story, 1/30-scale structure mounted on the Los Alamos electrodynamic shake table.

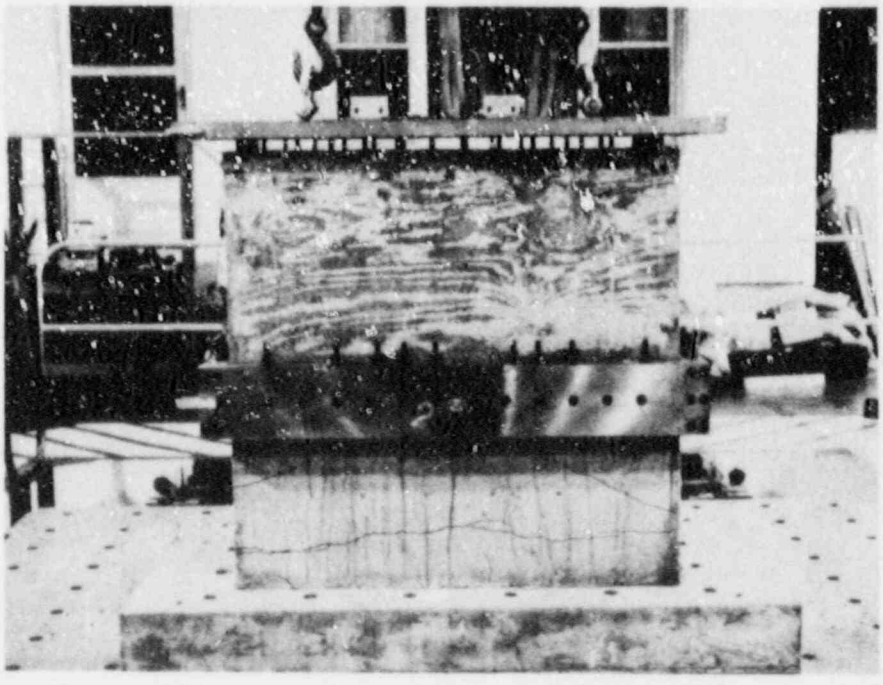

Fig. 15. A two-story, 1/10-scale structure mounted on the CERL servohydraulic shake table.

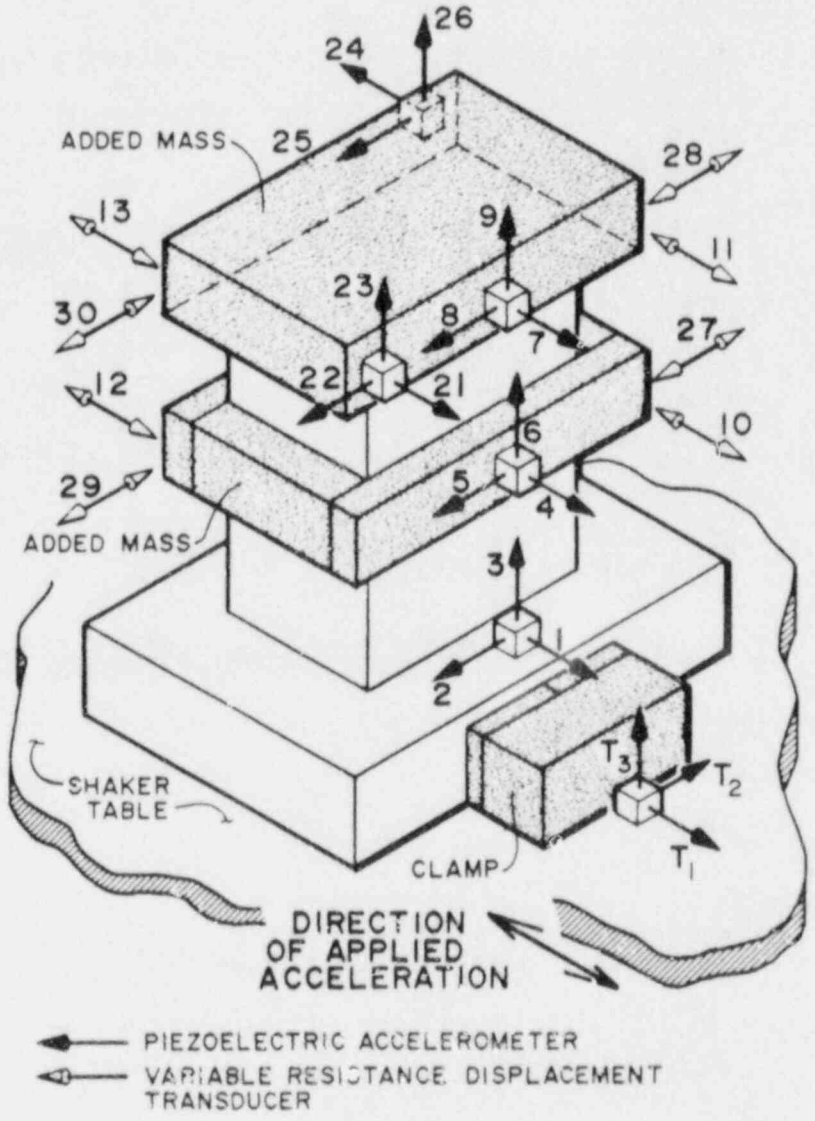

Fig. 16. Typical instrumentation package: simulated seismic tests.

pattern. All of the transducer signals were recorded on FM tape recorders so that they could be stored, digitized, and analyzed using all available data processing and computational facilities. Figures 17 and 18 illustrate the data taking and handling procedures.

Numerous still photographs were taken to document the post-test condition of the structure. Figure 19 is an example. The two tests at CERL on 1/10-scale structures were both recorded on video tape.

The test sequence was essentially the same for each structure, and that sequence is summarized in the following numbered paragraphs.

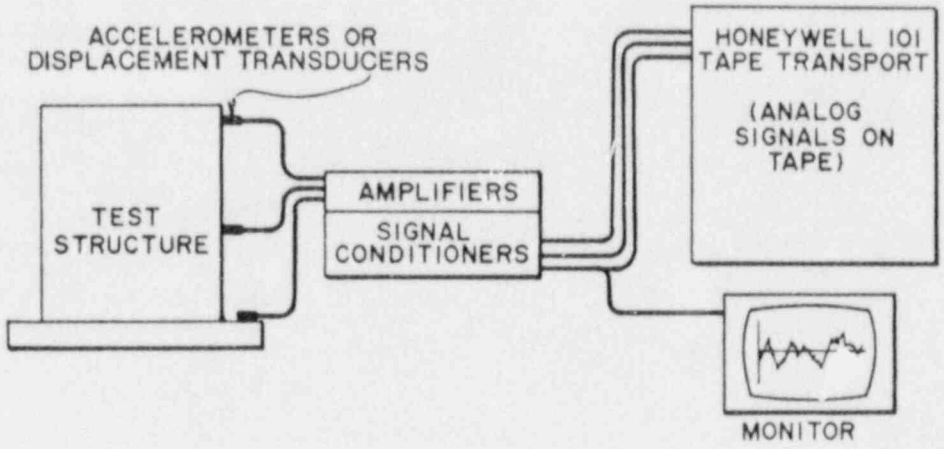

Fig. 17. Dynamic test data recording.

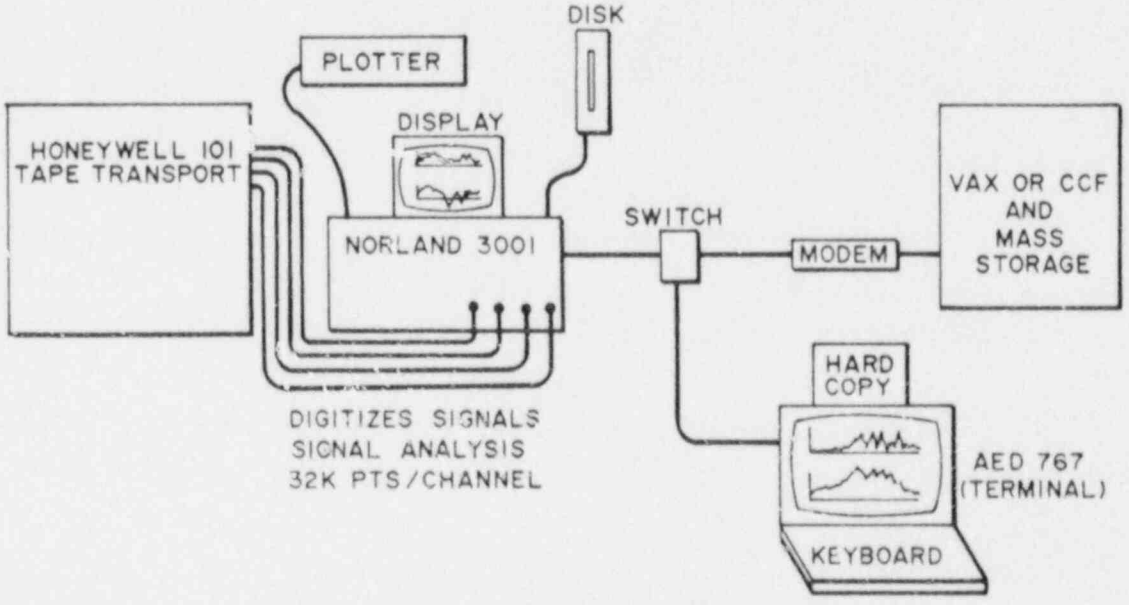

Fig. 18. Dynamic test data reduction.

D. Summary of Test Sequence

1. The test table was loaded with steel plates to approximate the weight of the structure to be tested. The seismic simulator was then driven with the command signal that was used during the proposed test. The base line-corrected accelerogram of the 1940 El Centro N-S, which was frequency scaled and used in all of these simulated seismic tests,* is shown in

*See Appendix C for a discussion of the scaling.

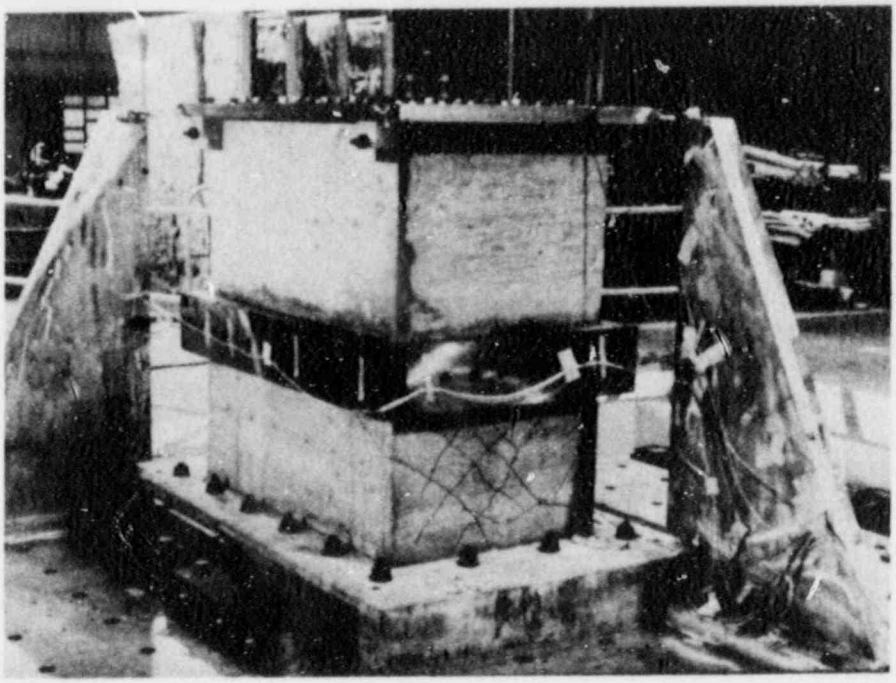

Fig. 19. Crack pattern, 1/10-scale structure.

Fig. 20. A series of tests was conducted during which the amplitude (peak table acceleration) was gradually increased. The purpose of tnis "dummy load" test was to allow the facility operator to establish the necessary system (electrical, servo, mechanical) transfer functions.which were used to properly control the facility during the actual test of the model structure.

2. The "dummy load" was removed and the structure to be tested was bolted to the test table. At this point, the steel plates that were added to the model to fulfill the scaling laws were not attached.
3. The "bare" model was instrumented (the number of accelerometers was fewer than shown in Fig. 16, but the accelerometers designated No.1, No. 4, and No. 7 in Fig. 16 were always used) and subjected to one or more low-level dynamic tests. The peak accelerations for a bare model were as low as 0.25 g up to 1.7 g. (This dynamic signal can be any low-level random wave form.) The purpose of this test was to obtain some information on the response of the bare model for comparison to the response of the final model, that is, one with masses added to fulfill the scaling laws. Figure 21 shows a typical transfer function plot obtained from one of these bare

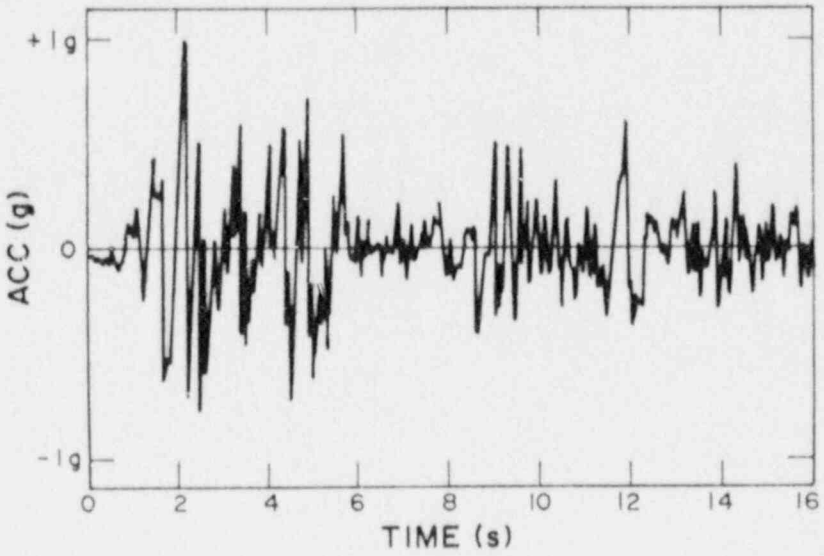

Fig. 20. 1940 El Centro N-S accelerogram (normalized to 1-g peak).

model tests. In this example (from the test of the 1/30-scale model, 3D-10), the transfer function is computed as first-floor response ($\ddot{X}_1$, accelerometer No. 4 in Fig. 16) over base input ($\ddot{Y}_1$ accelerometer No. 1 in Fig. 16). Notice that, for this two-story structure, two modal frequencies are identified--specifically 342 and 950 Hz.* The same modes can also be identified from the transfer function T.F. ($\ddot{X}_2/\ddot{Y}$), where $\ddot{X}_2$ is the second-floor response (that is, accelerometer No. 7 in Fig. 16).

4. Following these bare model tests, mass was added to each structure so that each structure would be a Case III scale model** of the assumed prototype structure, that is, a typical Category I, diesel generator building with a wall thickness of 30 in. It is important to note that this added mass does not represent equipment attached to the prototype; rather, it represents mass added to the model structures to fulfill the required similitude conditionsor scaling laws. The way in which these added masses were attached to the structures and the amount added at each story level are shown in Fig. 22. The appearance of the structures with added mass attached and ready for testing is shown in Figs. 14 and 15.

*Information beyond 1000 Hz is questionable because of frequency limitations in the data analysis procedure.
**See Appendix C.

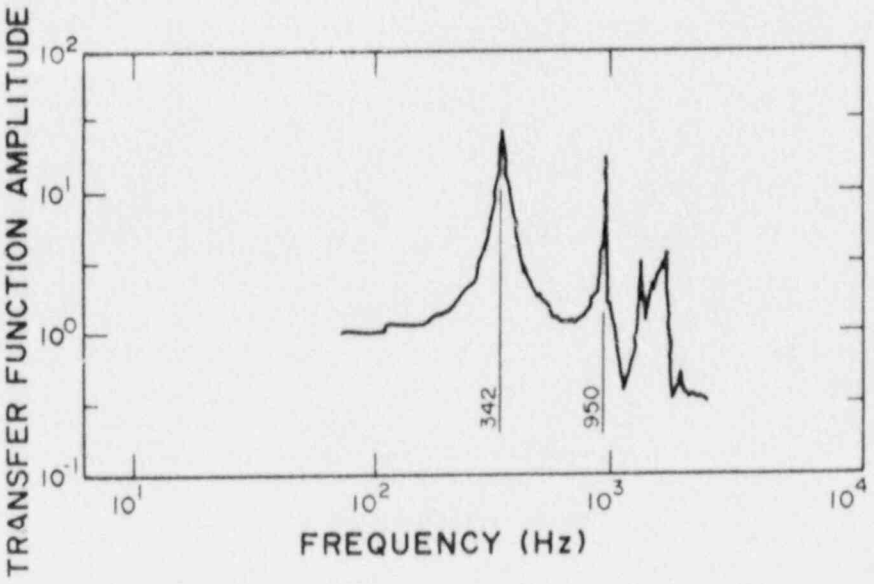

Fig. 21. Transfer function: 1/30-scale structure, no mass added.

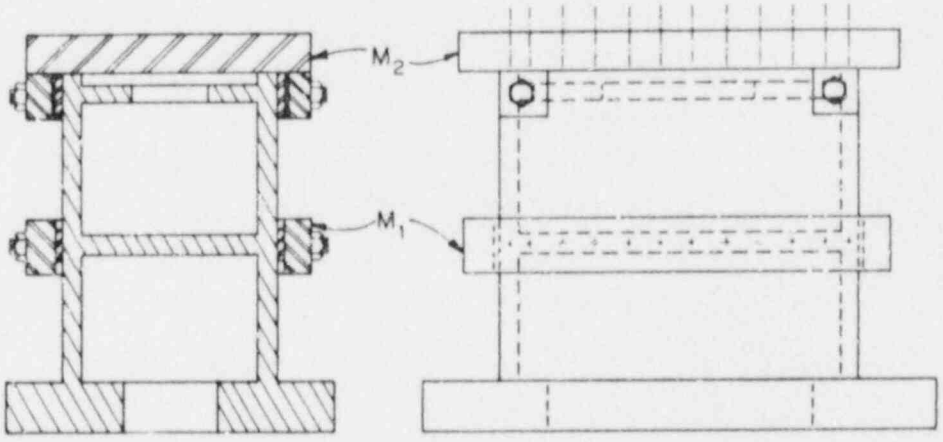

STRUCTURE	SCALE	M_1 (lbs)	M_2 (lbs)
3D-10-2	1/30	228	231
3D-11-2	1/30	228	231
3D-12-2	1/30	236	166
CERL 1	1/10	1285	1330
CERL 2	1/10	1285	906

Fig. 22. Method of attaching "added" mass.

5. The model, with the appropriate mass added, was then subjected to a series of simulated seismic events. The excitation was a properly frequency-scaled version of the 1940 El Centro N-S acceleration/time signal (see Fig. 20). It is important to note that, during the test series, the intent was to vary only one parameter, the peak input acceleration, $\ddot{Y}_{pk}$. This was the case since the object was to determine how modal frequency, damping, and floor response spectra vary with increasing seismic amplitude for a given earthquake. Ideally, frequency scaling and, hence, the energy content at each frequency remains constant during the test series on any model.*

We recognize that damage occurs progressively as the level of input acceleration is increased. Therefore, the results obtained from these tests particularly at the higher acceleration levels are probably not the same as might be obtained if a new or previously untested structure was used for each test. Clearly, the approach used here is a trade off between desired results and program cost.

The data from these simulated seismic tests were reduced in the following manner:

1. All of the tape recorded signals (accelerations and displacements) were digitized and stored in digital form. See Fig. 18.
2. All signals were inspected in the time domain, and peak displacements and accelerations were measured and recorded.
3. Desired floor response spectra (FRS) were computed, using a suitable program with the appropriate digitized acceleration vs time signal as input. The method is outlined in Fig. 23.

---

*In practice there is some variation in the frequency content, and energy distribution in the frequency domain, with variation in $\ddot{Y}_{pk}$. This is true because neither of the shaker facilities used (Los Alamos or CERL) nor any other facilities known to the authors are capable of exactly reproducing a transient control signal independent of that signal's amplitude. The ideal can be closely approached if we allow iteration between input signal and table response--that is, repetitive testing and input signal correction. However, repetitive testing further damages the structure, and, therefore, is not a suitable technique for these tests. The way in which this small but undesirable variation in frequency content is accounted for is discussed in more detail in Appendix B.

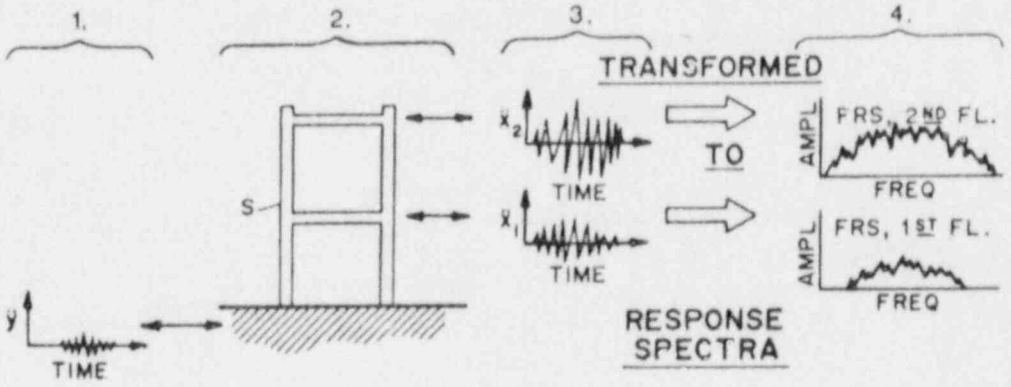

1. $\ddot{y}$ - The input acceleration signal applied to the base of the structure, S.
2. S - A physical structure or an analytical model of the structure.
3. $\ddot{x}_1$ and $\ddot{x}_2$ - The measured (for a physical structure) or computed (for an analytical model) acceleration response at the level indicated.
4. F.R.S.- Floor Response Spectra - The response spectra of the response signal $\ddot{x}_1$ and $\ddot{x}_2$.

Fig. 23. Computation of floor response spectra, FRS.

4. Modal frequencies and equivalent damping ratios were determined by transforming the appropriate signals from the time domain into the frequency domain and by computing transfer functions. The way in which these functions are used to determine modal frequencies and equivalent damping ratios is discussed in more detail in Appendix D.

IV. DISCUSSION OF RESULTS

A. Preliminary Static Tests: Single-Story, 1/30-Scale Structures

The basic purpose of the static tests conducted on the single-story, 1/30-scale structures was to determine the effective stiffness (K) of these structures. This is of utmost importance in seismic design and analysis, since the effective stiffness is one of the fundamental properties required for computation of a structure's modal frequency.

In seismic design or analysis of prototype structures, the usual practice is to compute the structural stiffness using mechanics-of-materials methods with the structure's geometry and the concrete's measured material properties. Typically, the initial uncracked stiffness (K) is computed using the relationship

$$\frac{1}{K} = \frac{1}{K_s} + \frac{1}{K_b} ,$$

where

K_s = $A_e G/h$,
K_b = $3EI/h^3$,
G = the concrete shear modulus = $E/2(1+\mu)$,
h = the story height,
A_e = the effective shear area,
E = the concrete elastic modulus,
I = the section moment of inertia, and
μ = Poisson's ratio, assumed to be 0.2 for concrete.

The computed stiffness clearly depends on the value used for elastic modulus of the concrete. Since concrete is not a linear elastic material, it is common civil engineering practice to specify a minimum concrete cylinder compressive strength, f'_c, and to measure the strength for each batch. An elastic modulus is computed based on this value of f'_c. The formula used is $E_c = 57{,}000\sqrt{f'_c}$, (for normal weight concrete, ACI 349-76, Sec. 8.3). In general, this value of E_c will correspond to a secant modulus through a point on the stress-strain curve that is about 45-50% of the value of the ultimate strength of the concrete. All of the computed stiffness values given in Table III for the single-story, 1/30-scale structures were computed using this method.

With the load vs deformation data available from the static tests of these structures, a measured value of stiffness is also available. However, as pointed out in the previous section of this report, these load vs deformation plots are not linear and, therefore, the way in which stiffness is measured is of considerable importance. The values of measured Stiffness given in Table III were determined as the secant modulus of the load vs deformation plot at a load level equal to 50% of the ultimate load (P_u).

The important conclusion is that, for these structures, the computed stiffnesses are between two and four times the measured stiffness (see the ratio column in Table III). If the computed values of stiffness were used to predict the modal frequency (f) of these structures, we would expect that the values would be too large by factors of $\sqrt{2.06}$ to $\sqrt{3.82}$, since modal frequency is

proportional to $\sqrt{K}$; this error, in turn, would effect all seismic response calculations.

B. Preliminary Dynamic Tests: Single-Story, 1/30-Scale Structures

The above conclusion was investigated with dynamic tests of single-story, 1/30-scale structures. Table IV compares the values of stiffness obtained from these dynamic tests with the values obtained by calculation using material properties $E = 57{,}000 \sqrt{f'_c}$. Note that structure 3D-5 was tested several times under a variety of conditions. If we consider only the transverse tests on the two structures, we find that the effective transverse dynamic stiffnesses are between 0.62 and 0.71 lb/in. x 10^6. These values are somewhat lower than those determined by static tests (0.76 - 1.14 lb/in. x 10^6, see Table III) but they are in far better agreement with static test results than they are with calculated values of stiffness (62.86 lb/in. x 10^6). We again concluded that the effective stiffness of these structures is considerably less than the value calculated using the usual methods. The data from the static and dynamic tests on the 1/30-scale structures are summarized in Fig. 24.

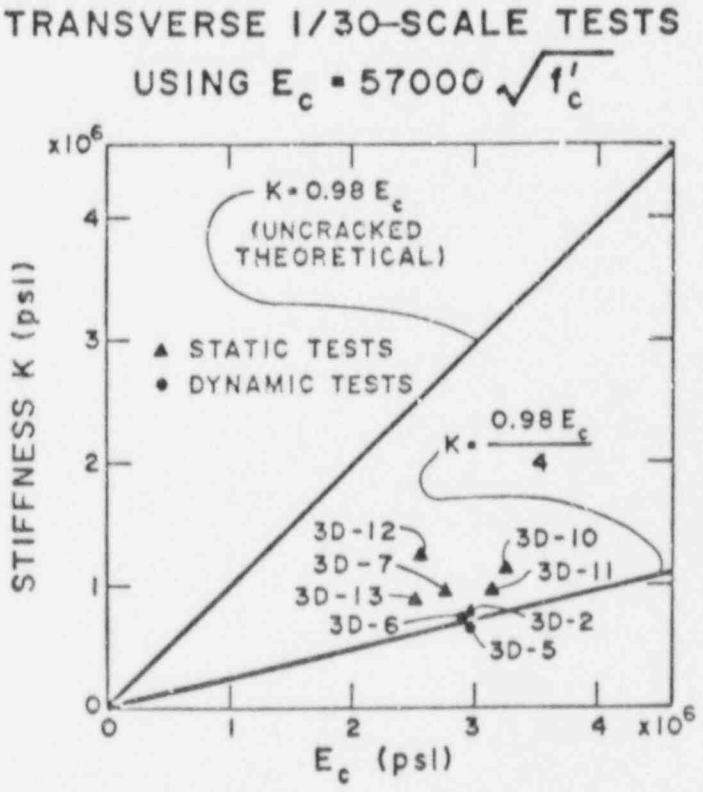

Fig. 24. Stiffness: 1/30-scale structures.

C. Simulated Seismic Tests: Two-Story, 1/30- and 1/10-Scale Structures

The simulated seismic tests involved five, two-story structures: three 1/30 scale and two 1/10 scale. These structures, designed as scale models of the assumed prototypical diesel generator building, are shown in Fig. 2. Table V lists these structures together with material properties and measured virgin modal frequencies.

These modal frequencies were determined from the transfer function plots, as explained in the previous section of this report. However, in these tests using a properly time- (or frequency-) scaled El Centro N-S accelerogram, the structure is so stiff relative to the frequency content of the input that the second mode response is very small. As a result, the second-mode frequency cannot be determined with any precision. For the same reason, the second-mode response is of little practical importance in this investigation of stiffness differences; therefore, only first-mode frequencies are tabulated.

These measured first-mode frequencies can be used in two ways;

1. The results from the 1/30-scale structure can be used to predict the behavior of the 1/10-scale structure.
2. The results from the tests on both structures can be used to predict the behavior of the assumed prototype, and these two predictions of prototype behavior can be compared.

Table VI compares the virgin first-mode frequency as measured on 1/10-scale structures to the values predicted from the values measured on the 1/30-scale structures; that is, the 1/30-scale structures are used as 1/3-scale models of the 1/10-scale structures. The authors believe that the data shown

TABLE V

TWO-STORY STRUCTURES USED IN SIMULATED SEISMIC TESTS

Structure				Virgin First Mode Frequency (f_1)	
(No).	Scale	f'_c (psi)	Test Location	No Mass Added (Hz)	Mass Added (Hz)
3D-10-2	1/30	2600	Los Alamos	342	104
3D-11-2	1/30	2890	Los Alamos	354	94
3D-12-2	1/30	N.A.	Los Alamos	270	94
CERL No. 1	1/10	3180	CERL	100	54
CERL No. 2	1/10	3330	CERL	94	53

in Table VI verify that these two structural sizes (1/30- and 1/10-scale) serve as adequate models for each other. Whether they are adequate models of the assumed prototype has, of course, not been proven in these tests.*

Table VII shows the predicted virgin first-mode frequency of the assumed prototype using all of the data from the 5 model tests. The predicted values for prototype first-mode frequency range from 7.5 - 11.8 Hz. This is a large scatter on a percentage basis. However, in any design using response spectra techniques, the difference between these values for the assumed first-mode frequency would have little effect. Furthermore, as the variation in measured modal frequencies of these 5 structures indicates, it would be impossible to build a prototype structure to obtain a precisely defined first-mode frequency.

Following the low-load level dynamic tests, each of the 5 two-story structures was subjected to a series of simulated seismic tests in which the peak acceleration input level ($\ddot{Y}_{pk}$) was progressively increased. The data from these tests make it possible to determine the following:

1. the way in which effective stiffness (K) and effective damping (ζ) vary with acceleration input level ($\ddot{Y}_{pk}$),

---

*During FY 1985, a new configuration will be tested. Two sizes of this configuration will be fabricated and seismicly tested. The smaller structure will use microconcrete and wire reinforcement and the larger will use regular aggregate concrete and standard reinforcement. These tests should address the feasibility of scaling to prototype size.

TABLE VI

COMPARISON OF 1/30- and 1/10-SCALE RESULTS

(Virgin, First-Mode Frequencies)

Test Condition	Structure	Measured	Predicted from* 3D-10-2	3D-11-2	3D-12-2
No Mass Added	CERL No. 1	100	$\{342\sqrt{3} = 114\}$	$\{354\sqrt{3} = 118\}$	$\{270\sqrt{3} = 90\}$
	CERL No. 2	94			
Mass Added	CERL No. 1	54	$\{104\sqrt{3} = 60\}$	$\{94\sqrt{3} = 54\}$	$\{94\sqrt{3} = 54\}$
	CERL No. 2	53			

*With no mass added, the frequency scale relating the 1/30- and the 1/10-scale structures is 3; with added mass, the scale is $\sqrt{3}$. See Appendix C.

TABLE VII

PREDICTION OF PROTOTYPE VIRGIN FIRST-MODE FREQUENCY

Model No. Predicted From	Scaling Method* $f_{1P} = f_{1M} \times N_f$†	Predicted Prototype First-Mode f_{1P}(Hz)
3D-10-2		
No Mass Added	$f_{1P} = 342 \times 1/30$	11.4
Mass Added	$f_{1P} = 104 \times 1/11.8$	8.8
3D-11-2		
No Mass Added	$f_{1P} = 354 \times 1/30$	11.8
Mass Added	$f_{1P} = 94 \times 1/11.8$	8.0
3D-12-2		
No Mass Added	$f_{1P} = 270 \times 1/30$	9.0
Mass Added	$f_{1P} = 94 \times 1/12.2$	7.7
CERL No. 1		
No Mass Added	$f_{1P} = 100 \times 1/10$	10.0
Mass Added	$f_{1P} = 54 \times 1/6.8$	7.9
CERL No. 2		
No Mass Added	$f_{1P} = 94 \times 1/10$	9.4
Mass Added	$f_{1P} = 53 \times 1/7.04$	7.5

*See Appendix C for a discussion of scaling.

† f_{1P} - first-mode frequency of the prototype.
f_{1M} - first-mode frequency of the model.
N_f - the frequency scale factor, defined as f_P/f_M.

2. the level of ($\ddot{Y}_{pk}$) beyond which the stiffness and damping begin to undergo significant change,
3. the level of ($\ddot{Y}_{pk}$) required to produce failure of the structure, and
4. the way in which floor response spectra vary with the level of input acceleration.

Table VIII shows the test sequence used for each of the 5 structures.

The data presented in Table VIII have been plotted in Figs. 25 and 26 to show the variation in first-mode frequency (f_1) with input acceleration level ($\ddot{Y}_{pk}$).*

Figure 25 shows the data taken during FY 83 from tests on two 1/30-scale models (3D-10-2 and 3D-11-2) and one 1/10-scale model (CERL No. 1). Figure 26 shows the data taken during FY 84 from tests on an additional 1/30-scale model (3D-12-2) and on a second 1/10-scale model (CERL No. 2). These FY 84 tests differed from the FY 83 tests in two respects: (1) the attached masses were adjusted slightly (mass added to the second-story was decreased) to better represent the equivalent distributed mass, and (2) the drive signal ($\ddot{Y}$ vs t) used in the 1/30-scale test was refined to better match the drive signal used in the 1/10-scale test. As can be seen by comparing Figs. 25 and 26, these two modifications had only minor effect and all of the data could have been plotted on a single sheet.

The solid lines shown in Figs. 25 and 26 are not "best fit" curves for the data points shown. Rather, they were added to suggest the following design application of these data:

1. All models suggest that the assumed prototype diesel generator building will have a virgin first-mode frequency of 7.5 - 8.8 Hz.
2. When subjected to the El Centro N-S earthquake of peak magnitude up to 0.2 g, the prototype will respond with this virgin first-mode frequency.

---

*All of the data presented in Table VIII from the several tests can be plotted on the same sheet by multiplying f_1 by the frequency scale (N_f) and $\ddot{Y}_{pk}$ by the acceleration scale ($N_{\ddot{Y}}$). This is true since, under these test conditions (appropriate masses added to each model and the base motion properly frequency and acceleration scaled), the 1/30-scale structure is a 1/3-scale model of the 1/10-scale structure, and both structures are models of the assumed prototype. In addition, when plotted in this manner, prototype behavior, predicted by each model, is shown directly.

TABLE VIII

TEST SEQUENCE

(Two-Story Structures, Simulated Seismic, with Added Mass)

Structure	Test (No.)	Input Level $\ddot{Y}_{pk}$(g)	Measured First Mode Frequency f_1(Hz)	Remarks
3D-10-2				
1/30-Scale	1	1.5	104	1
Los Alamos	2	5.3	80	2
3D-11-2	1	<0.5	94	1,3
1/30-Scale	2	0.75	93	--
Los Alamos	3	1.0	92	--
	4	1.5	90	--
	5	8.2	63	2
	6	<0.5	71	4
3D-12-2	1	0.4	94	1
1/30-Scale	2	0.75	93	
Los Alamos	3	1.35	91	
	4	3.17	91	
	5	4.09	90	
	6	6.26	87	
	7	6.41	85	
	8	11.86	69	
	9	11.23	64	
	10	20.0	--	5
CERL #1	1	0.7	54	1
1/10-Scale	2	1.2	54	
CERL	3	2.0	51	
	4	2.7	50	
	5	3.5	49	
	6	4.7	47	
	7	7.0	44	
	8	9.0	41	
	9	10.0	38	
	10	12.0	24	
	11	16.0	--	6
CERL #2	1	0.83	53	1
1/10-Scale	2	0.74	53	
CERL	3	1.85	50	
	4	3.94	48	
	5	5.43	46	
	6	6.86	39	
	7	8.28	33	
	8	11.3	25	
	9	17.0	--	7

Remarks:

1. Low-level tests with no mass added preceded this test.
2. End of test--shaker displacement limit reached. Structure did not fail.
3. A wide-band test (rather than simulated seismic).
4. A wide-band, low-level test to establish irreversible change; note that f_1 only partially "recovers."
5. Structure failed by shear at junction of base to first-story wall.
6. Structure failed by shear of first-story wall; see Fig. 19.
7. Same as #5 above and walls completely separated from base.

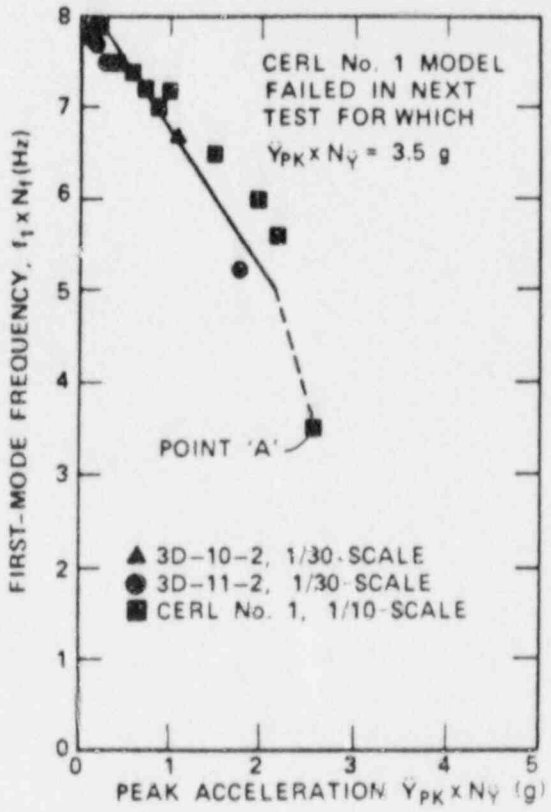

NOTES:

FOR 1/30-SCALE, $N_f = 1/11.8$, $N_{\ddot{Y}} = 1/4.6$

FOR 1/10-SCALE, $N_f = 1/6.8$, $N_{\ddot{Y}} = 1/4.6$

EXAMPLE:

AT POINT 'A' CERL TEST No.1

$f_{1_{PROT.}} = 24 \times 1/6.8 = 3.5$ Hz

$\ddot{Y}_{PK_{PROT.}} = 12 \times 1/4.6 = 2.6$ g

Fig. 25. Variation in first-mode frequency, FY 1983 tests.

3. If subjected to a peak intensity of greater than 0.2 g, the prototypes will respond with a reduced effective first-mode frequency. The greater the amplitude, the lower the effective modal frequency. This implies that the floor response spectra for a given acceleration-vs-time excitation (in this case the El Centro, N-S) will vary with peak amplitude of input. This is contrary to the usual linear design assumption.
4. Inspection of the various models indicate that these reductions in modal frequency will occur without visible signs of cracking;

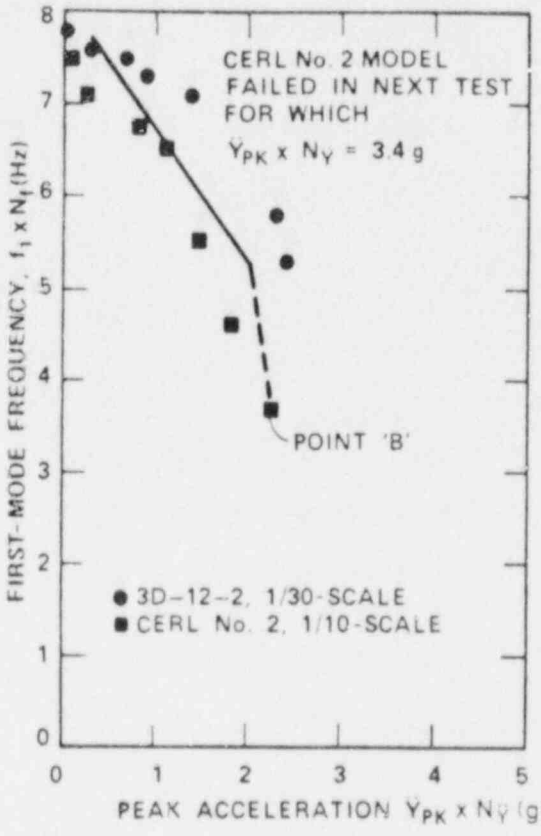

NOTES:

FOR 1/30 SCALE, $N_f = 1/12.2$, $N_{\ddot{Y}} = 1/4.95$

FOR 1/10 SCALE, $N_f = 1/7.04$, $N_{\ddot{Y}} = 1/4.95$

EXAMPLE:

AT POINT 'B' CERL TEST No. 2

$f_{1_{PROT}} = 25 \times 1/7.04 = 3.5$ Hz

$\ddot{Y}_{PK_{PROT}} = 11.3 \times 1/4.95 = 2.3$ g

Fig. 26. Variation in first-mode frequency, FY 1984 tests.

5. Low-level, wide-frequency-band diagnostic tests, which were performed between the seismic tests, indicate that any reduction in the effective modal frequency will be permanent.
6. The assumed prototype diesel generator building would not fail (significant visual cracking and breaking loose from the foundation at the lower walls) until the amplitude exceeded 2.5 g.

Figure 19 illustrates the crack pattern on one of the lower-story end walls of a 1/10-scale model after the test. The orientation of the cracks is consistent with the predominant development of shear stress in the end wall.

This diagonal crack pattern was not visible in the 1/30-scale models, probably because of the lower ultimate elongation of the reinforcement used in the 1/30-scale models, (4% for 1/30 scale, 13.1% for 1/10 scale).

The quantification of damping associated with the response of structures subject to transient loads that produces nonlinear and/or inelastic responses has proved to be a very difficult problem. This is especially true for reinforced concrete structures for which the exact damping mechanism is unknown (that is, is damping viscous, structural, Coulomb, or perhaps a combination of all three?)

Because one of the objectives of this program is to improve our ability to analyze structures loaded into their inelastic region, we have attempted to characterize and quantify damping in a way that will be most useful in the analysis process. Therefore, because most analysis methods utilize response spectra and computations that involve equivalent viscous damping ratios, these tools and concepts are used in our evaluation and quantification of damping (ζ).*

Two methods of quantifying damping have been used. The first method will be referred to as the "Floor Response Spectra (FRS) Matching Technique" and the second method as the "Transfer Function Analysis Technique (TFAT)."

The "FRS Matching Technique" involves the use of a computer model and iteration with different values of damping ratio (ζ) until the computer-generated FRS "match" the FRS generated from response data measured during a test at a given input acceleration level ($\ddot{Y}_{pk}$).

The TFAT involves plotting the transfer function (TF) of the response acceleration, $\ddot{X}_1(t)$ or $\ddot{X}_2(t)$, to the input, $\ddot{Y}(t)$, at a given input acceleration level ($\ddot{Y}_{pk}$). The real part of this transfer function is then examined to determine the damping ratio (ζ).**

In Fig. 27 the computed values of damping ratio, (ζ) from tests of these models, are plotted vs the peak acceleration level ($\ddot{Y}_{pk}$) of the test for which that value of damping ratio applies. All of the values, except the 2 points

---

*The use of and assigning values for "equivalent viscous damping ratios (ζ)" should not be taken to imply that the damping mechanism is viscous. Rather this value use is only an attempt to assign an appropriate value to a term that is needed in response spectra and other methods of analysis.
**These methods are discussed in more detail in Appendices D and E.

indicated as FRS Matching Technique, were determined using the TFAT. There is considerable scatter in the data, but the authors believe that the following observations are justified:

1. These 3 models respond to inputs with magnitude of less than 4 g s as if they had equivalent viscous damping ratios of 5.5% - 8%.
2. For input magnitudes of 4 - 9 g, the effective viscous damping tends to increase.
3. At input magnitudes greater than 9 g (where all of the models are known to be close to failure), the damping is uncertain.

The next important issue concerning damping is whether or not the damping effects are distorted in the models as compared within prototype. If so, how are the effective damping ratios measured in these models related to the effective damping in the prototype? As demonstrated in Ref. 7, we would expect that damping forces are distorted between the 1/30- and the 1/10-scale models, but only if the damping mechanism is viscous. Analysis of the data plotted in Fig. 27 confirms that the damping mechanism is not viscous and, therefore, the values of equivalent damping ratios determined from these model tests are expected to apply to the prototype structure.*

In connection with these observations, it is important to note that, since in both models (1/30- and 1/10-scale), acceleration is scaled by a factor of approximately 5, the region of noticeably increasing damping (region A - B in Fig. 27) corresponds to input amplitude ($\ddot{Y}_{pk}$) to the prototype in excess of 1-g peak acceleration.

The way in which a structure modifies the input base motion is of great interest, and this information is usually expressed in terms of FRS. The way in which FRS is defined is shown in Fig. 23. The usual practice is to assume that the structure is a linear system. With this assumption, for a given structure subjected to an acceleration signal of a given frequency content, the FRS is a constant; that is, FRS is independent of amplitude of the input signal. As pointed out in the preceding paragraphs, the structures being discussed in this report have been loaded into their nonlinear/inelastic range. Therefore, it is important to determine how this nonlinear/inelastic response affects the FRS.

---

*The details of this analysis are included in Ref. 7.

This has been done using the data obtained from the tests of a 1/10-scale structure (CERL No. 1); however, frequencies and accelerations have been scaled to prototype values, as was done in Figs. 25 and 26. Figure 28 shows the first- and second-floor-response spectra (FRS_1 and FRS_2) computed from the measured response ($\ddot{X}_1$ and $\ddot{X}_2$) of the 1/10-scale structure during a low g level test (1.3 g on the model, 0.26 g on the prototype). As would be expected, the maximum amplification occurs in the region of the structure's first-mode frequency (f_1 = 54 Hz; f_1/N_f = 7.9 Hz). Because this is a stiff structure (relative to the frequency content of the input, that is, the 1940 El Centro N-S) the second and higher modes produce relatively insignificant amplifications. Now if this structure remained unaltered at higher input level tests, we would expect that the FRS would remain as shown in Fig. 28. We know, of course, from our previous analysis of shifts in modal frequency at higher input levels, that the structure undergoes progressive decrease in stiffness at the higher input levels. Therefore, we anticipate that the floor response spectra will vary with input level.

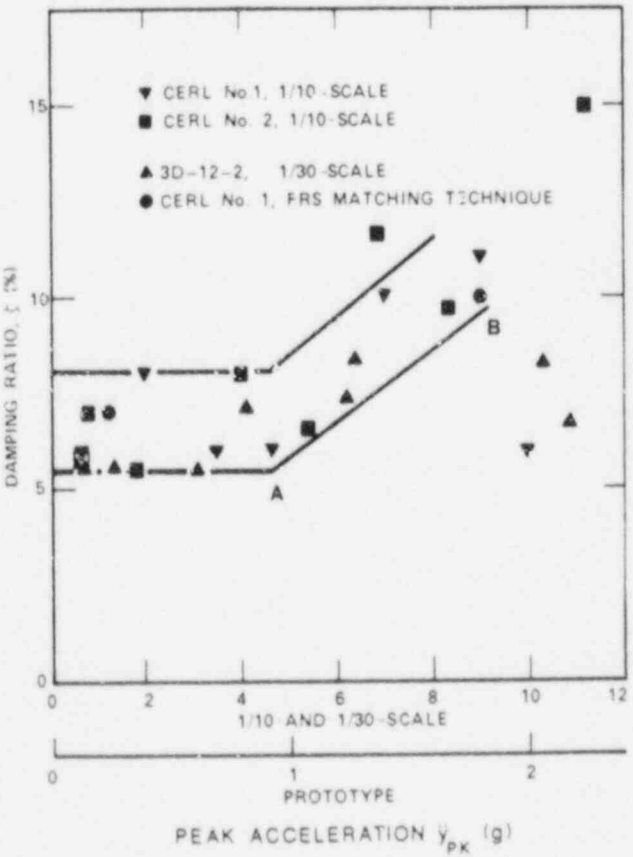

Fig. 27. Measured damping ratios.

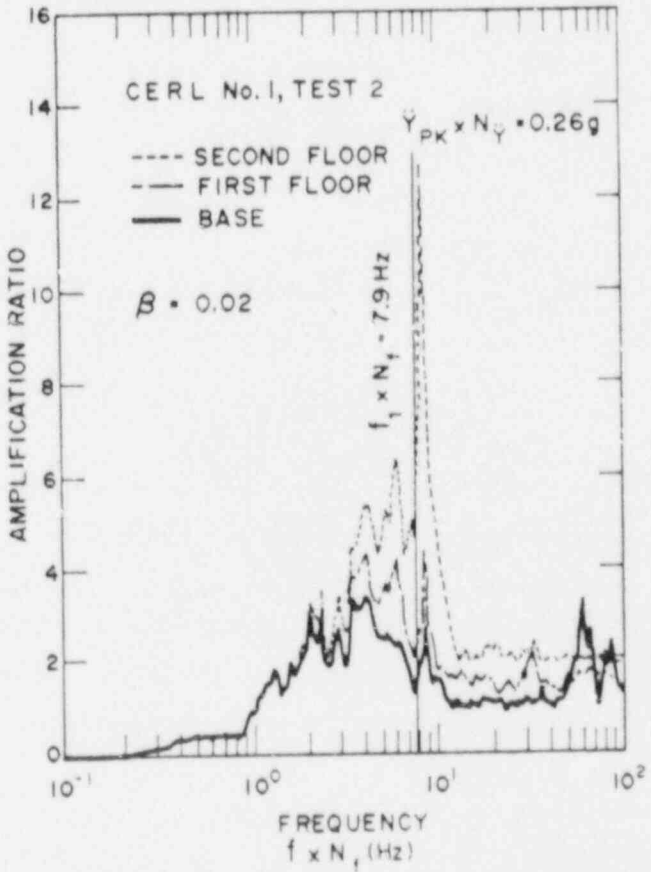

Fig. 28. Floor response spectra: $\ddot{Y}_{pk}/N\ddot{y}$ = 0.26 g.

This is indeed the case, as can be seen by comparing Figs. 29, 30, and 31 with Fig. 28. As the base acceleration input level is increased and the effective first-modal frequency is decreased, the frequency region over which amplification occurs is down shifted and, in this particular case, the magnitude of peak amplification is decreased. Note, however, that as the first mode frequency is decreased toward the frequency region in which the input signal is maximum, the amplification of the response in this region is increased and, if the first-mode frequency should be reduced so as to exactly correspond to one of the frequencies at which the input level reaches a peak, the maximum magnification of response could, of course, be increased.

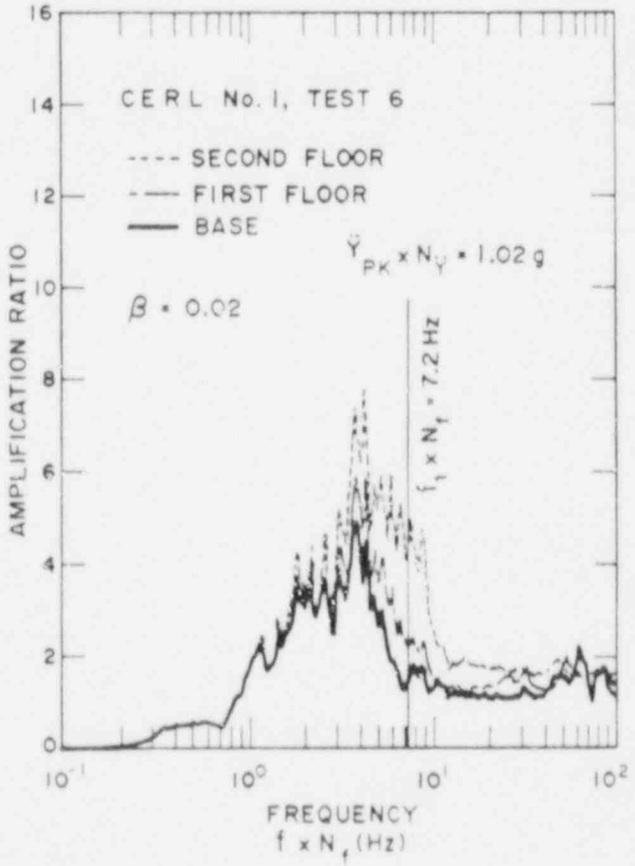

Fig. 29. Floor response spectra: $Y_{pk}/N\ddot{y}$ = 1.02 g.

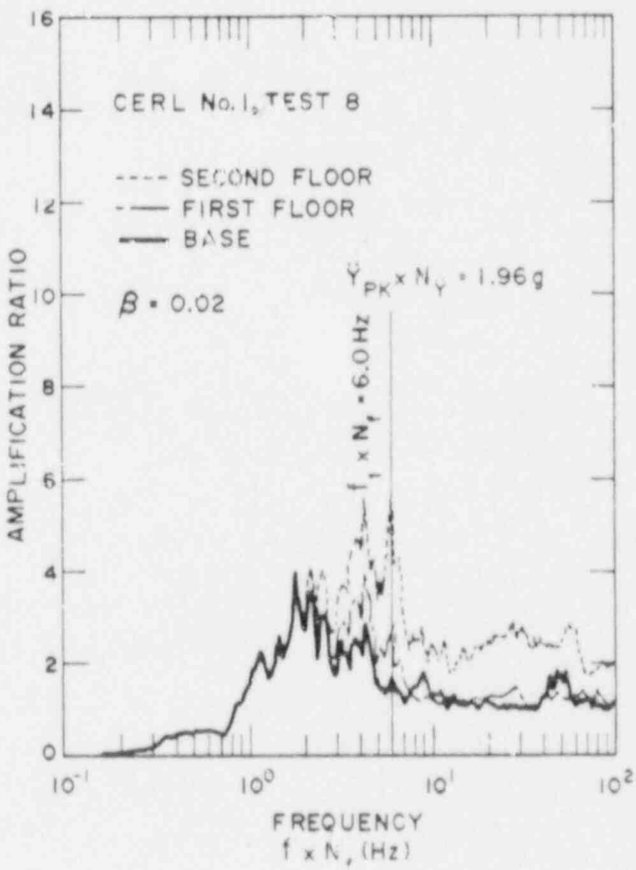

Fig. 30. Floor response spectra: $Y_{pk}/N\ddot{y}$ = 1.96 g.

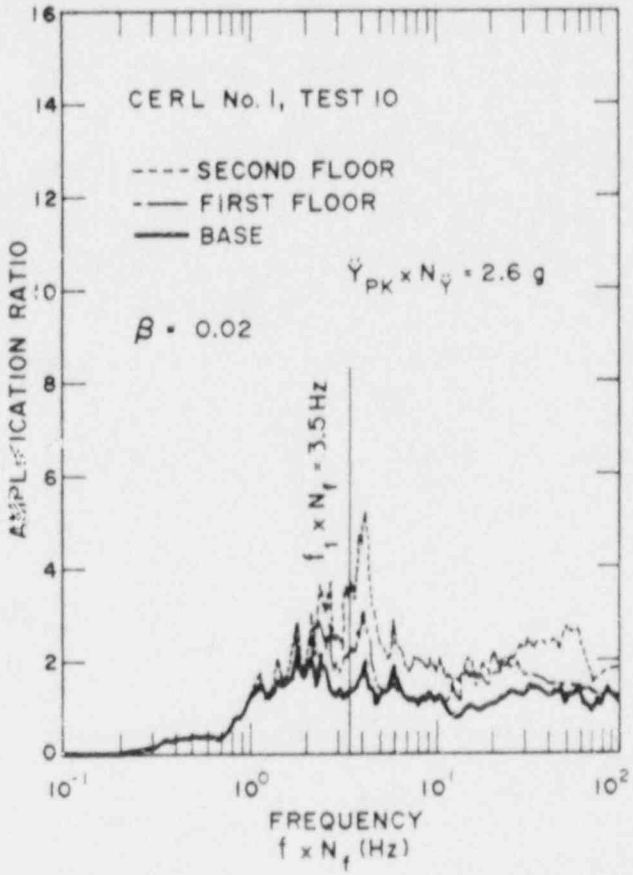

Fig. 31. Floor response spectra: $\ddot{Y}_{pk}/N_{\ddot{y}} = 2.6$ g.

V. CONCLUSIONS AND RECOMMENDATIONS

Based on the data presented in this paper, on the data from the isolated shear wall tests (see Ref. 2), and upon recent studies made by other investigators,[8,9] the authors believe that the actual stiffnesses of prototypical, Category I structures may be considerably less than the values computed using the usual design procedures. We recognize that, because all of these tests involve small structures (models), the observed smaller values of stiffness could be structure-size related.

The Technical Review Group (TRG) for this program has recommended that the effect of using "model" or microconcrete material be evaluated. A program to resolve this issue is being planned for FY 1985.

We believe that the prototype structures could experience considerable nonlinear and inelastic response without showing visible signs of cracking. When cracking appears, the structure may have experienced large nonlinear and

inelastic response, and the effective structural stiffness may already be significantly reduced. The input acceleration level required to produce this condition is, however, very large. For the prototypical diesel generator building subjected to the 1940 El Centro N-S earthquake investigated in this study, the cracking and the very large reduction in first-mode frequency would be expected at an input acceleration level of 0.2 g or higher.

The measured values for effective viscous damping ratios (from 5.5 - 8%) are in reasonable agreement with values currently recommended for reinforced concrete design.[10] Although our studies indicate that at higher load levels, the damping increases, the load level at which this increase occurs in the structure investigated (>1 g) is so large that it is doubtful if this increase in damping is of any value in design for realistic loading.

The reduction of first-mode frequency, which is associated with the reduction in effective stiffness, retunes the structure relative to the input and, as a result, the floor-response spectra are different at different levels of input acceleration. The way in which this affects equipment mounted at a given level depends upon its mounted frequency relative to the original structural first-mode frequency. In general, we can say that, if equipment is mounted such that its resonance value is less than the original structural first-mode frequency, it could be tuned to the structure's resonance during high-seismic-load response.

We believe that the results presented in this report demonstrate the potential value of 1/30- or 1/10-scale-model tests. The 1/30-scale models appear to be appropriate to investigate a number of design and test parameters of interest, that is, they are useful in sensitivity studies. The relative low cost and convenience of the smaller models allows a larger number of parameters to be investigated. However, for very important parameters or for those that may be judged to be very sensitive to size effects, larger scales are appropriate.

REFERENCES

1. E. G. Endebrock, R. C. Dove, and C. A. Anderson, "Margins to Failure - Category-I Structures Program: Background and Experimental Program Plan," Los Alamos National Laboratory report LA-9030-MS, NUREG 2347 (September 1981).

2. E. G. Endebrock, R. C. Dove, and W. Dunwoody, "Analysis and Tests on Small-Scale Shear Walls - FY-82 Final Report," Los Alamos National Laboratory report, LA-10443-MS, NUREG/CR-4274 (September 1985).

3. N. M. Newmark and W. J. Hall, "Procedures and Criteria for Earthquake Resistant Design," in Building Practices for Disaster Mitigation, R. Wright, S. Kramer, and C. Culver, Eds. (Center for Building Technology, National Bureau of Standards, Washington, D.C. 20234, February 1973).

4. C. K. Chen, R. M. Czarnecki, and R. W. Scholl, "Destructive Vibration Test of a Four-Story Concrete Structure," Douglas McHenry International Symposium on Concrete and Concrete Structure, American Concrete Institute, Detroit, Michigan (1978). 607-637.

5. T. V. Galambos, and R. L. Mayes, "Dynamic Tests of a Reinforced Concrete Building," Washington University of Research report No. 51, Structural Division, St. Louis, Missouri (June 1978).

6. Adrian Pauw, "Static Modulus of Elasticity of Concrete as Affected by Density," J. of the Amer. Concrete Inst., V. 32, No. 6, December 1960 (Proceedings V. 57), A.C.I. Detroit, Michigan, pp. 679-687.

7. Richard C. Dove and Joel G. Bennett, "Scale Modeling of Reinforced Concrete Category I Structures Subjected to Seismic Loading," Los Alamos National Laboratory report LA-10624-MS, NUREG/CR-4474 (January 1986).

8. J. Gauvain, et. al, "Tests and Calculations of the Seismic Behavior of Concrete Structures," Proceedings, 5th Conference on Structural Mechanics in Reactor Technology, Berlin August 1979.

9. H. Umemura, et. al., "Aseismic Characteristics of RC Box and Cylinder Walls," Proceedings, Sixth World Conference on Earthquake Engineering, New Delhi, India, 1976.

10. NRC Regulatory Guide, 1.60, (U.S. Nuclear Regulatory Commission, Washington, D.C.).

APPENDIX A

STRUCTURES CONSTRUCTED - MATERIAL PROPERTIES

TABLE A-I

STRUCTURES CONSTRUCTED AND TESTED DURING FY 1983 AND 1984

No.	Structure Scale	No. of Stories	Type of Test*	Location of Test	Purpose of Test**
3D-2	1/30	1	Static, M,T	Los Alamos	A
3D-4	1/30	1	Static, M,L	Los Alamos	A
3D-8	1/30	1	Static, C,T	Los Alamos	A
3D-9	1/30	1	Static, C,L	Los Alamos	A
3D-5	1/30	1	Seismic, L&T	Los Alamos	B
3D-6	1/30	1	Seismic, T	Los Alamos	B
3D-7	1/30	1	Static, M,T	Los Alamos	A&C
3D-10	1/30	1	Static, M,T	Los Alamos	A&C
3D-11	1/30	1	Static, M,T	Los Alamos	A&C
3D-12	1/30	1	Static, M,T	Los Alamos	A&C
3D-13	1/30	1	Static, M,T	Los Alamos	A&C
3D-19	1/30	1	Static, M,T	Los Alamos	A&D
3D-20	1/30	1	Static, M,T	Los Alamos	A&D
3D-10-2	1/30	2	Seismic, T	Los Alamos	E
3D-11-2	1/30	2	Seismic, T	Los Alamos	E
3D-12-2	1/30	2	Seismic, T	Los Alamos	E
CERL-1	1/10	2	Seismic, T	CERL	E&F
CERL-2	1/10	2	Seismic, T	CERL	E&F

*M - Monotonic Test.
C - Cyclic Test.
T - Transverse; load parallel to short dimensions.
L - Longitudinal; load parallel to long dimension.
Seismic - Scaled version of El Centro (1940) N-S accelerogram.

**A - Comparison of measured stiffness to computed value.
B - Measure single-story resonant frequency, check effective stiffness and effective mass.
C - Model structures that have different reinforcement embedment depths in the base slab; tested at 3, 6, 12, and 24 weeks after casting to determine the effect of steel embedment on the failure modes and aging effects on the initial stiffness.
D - Model structures tested immediately after removal from moist chamber to determine initial stiffness before any drying occurs.
E - Test to progressively larger inputs, track changes in modal frequency, damping, and shifts in floor response spectra.
F - Check scalability of results, i.e., from 1/30- to 1/10-scale structures.

TABLE A-II

MATERIAL PROPERTIES, TEST STRUCTURES

Structure Number	Concrete f'_c (psi)	Concrete f_t (psi)	Concrete E* (psi x 10^6)	Reinforcement σ_y (psi)	Reinforcement σ_{ULT} (psi)	Reinforcement E** (psi x 10^6)	Maximum Elongation (%)
30-2	2700	350	2.3	***59,000	66,500	26.9	7.7
30-4	3320	340	2.6	***59,000	66,500	26.9	7.7
30-5	2620	330	2.4	†42,700	53,100	25.6	4.0
30-6	2500	310	2.4	†42,700	53,100	25.6	4.0
30-7	2350	430	2.5	†42,700	53,100	25.6	4.0
30-8	2300	310	2.4	†42,700	53,100	25.6	4.0
30-9	2690	350	2.5	†42,700	53,100	25.6	4.0
30-10	3270	440	N.A.	†42,700	53,100	25.6	4.0
30-11	3090	400	N.A.	†42,700	53,100	25.6	4.0
30-12	2050	270	N.A.	†42,700	53,100	25.6	4.0
30-13	2040	400	N.A.	†42,700	53,100	25.6	4.0
30-19	4700	470	N.A.	†42,700	53,100	25.6	4.0
30-20	4300	440	3.3	†42,700	53,100	25.6	4.0
30-10-2	2600	340	2.5	†42,700	53,100	25.6	4.0
30-11-2	2890	420	N.A.	†42,700	53,100	25.6	4.0
30-12-2	2780	390	2.8	†42,700	53,100	25.6	4.0
CERL-1	3180	430	2.8	††42,400	50,000	28.5	13.1
CERL-2	3330	375	2.6	††42,400	50,000	28.5	13.1

* Measured in compression test, initial tangent modulus.
** Measured in tensile test.
*** Lot 2 wire.
† Lot 3 wire.
†† Model deformed wire purchased from Const. Tech. Lab., Portland Cement Assn., D-1-1.

APPENDIX B

LOS ALAMOS AND CERL SHAKER CHARACTERISTICS

The preliminary dynamic and the simulated seismic tests of the 1/30-scale structures were conducted on the electrodynamic vibration test facility located at K-site, Los Alamos National Laboratory, Los Alamos, New Mexico. The electrodynamic vibrator used was an 18,000-lb force machine manufactured by the M. B. Electronic Corporation. The shaker drives a uniaxial (horizontal), 4 ft x 4 ft, magnesium alloy, slip table mounted on Team hydrostatic bearings.

The system is capable of:

26 g peak acceleration (no load on table),

100 in./s peak velocity, and

± 0.5 in. displacement

over a frequency band of 5 - 5,000 Hz. For the FY 1983 tests, the system was programmed and controlled by a Hewlett Packard 5427A digital vibration control system. For the FY 1984 tests, a Gen Rad vibration control system was used. Both of these systems provide for transient vibration (i.e., simulated seismic) control.

Since the tests discussed in this report were completed, the Los Alamos facility has been upgraded by replacing the 18,000-lb force shaker with a 36,000-lb force, Unholtz-Dickie shaker.

The 1/10-scale structures discussed in this report were tested on the servohydraulic vibration test facility operated by the Construction Engineering Research Laboratory (CERL) at Champaign, Illinois. This is a biaxial machine (one horizontal axis plus vertical), but only single axis motion (horizontal) was used in these tests. Test items are mounted on 12 ft x 12 ft welded aluminum table that can support a dead weight of 810,000 lb.

The system is capable of:

A. Vertical Motion

810,000 lb force,

Approximately 50-g peak acceleration (no load on table),

27 in./s peak velocity, and

± 1.375 in. displacement.

B. Horizontal Motion

450,000 lb force,

Approximately 40-g peak acceleration (no load on table),

32 in./s peak velocity, and

± 2.75 in. displacement.

The system is controllable over a frequency range of 0-200 Hz. The system is programmed and controlled by a Gen Rad vibration control system that allows for transient vibration control.

APPENDIX C

SCALING OF THE 1/30- AND 1/10-SCALE STRUCTURE

The 1/30-scale structures (1-in. wall thickness) and the 1/10-scale structures (3-in. wall thickness) were designed, constructed, and tested so that each size of structure was a Case III scale model of the assumed prototype diesel generator building (30-in. wall thickness). In addition, the smaller (1/30-scale) structures were 1/3-scale, Case II models of the larger (1/10- scale) structures. The various types of modeling (Case I, Case II, and Case III) are discussed in detail in Ref. 7, with the scaling laws that must be fulfilled for each case. In this appendix, the design of the structures and test conditions, so that the scaling laws are fulfilled, is outlined.

The structures being considered are shown in Fig. C-1. All model structures were constructed using microconcrete and steel reinforcement. It was intended that the concrete and steel material properties would be the same as those of the prototype materials. For the 1/30-scale structure, the length scale is $\bar{N}_h = 30$; and for the 1/10-scale structure, $\bar{N}_h = 10$. The length scales were selected (i.e. the sizes selected) as the smallest size (1/30 scale) that we believed we could fabricate with good modeling of the reinforcement detail and as the largest size (1/10-scale) that could be tested to failure on an existing seismic simulator.

It was decided that each structure was to serve as a Case III model of the assumed prototype. This decision was made because it was necessary to have control of the acceleration scale, $N_{\ddot{y}}$, the mass scale, N_m, and the time scale, N_t, if these models were to be tested to failure on the available seismic simulators. For both structures (1/30-scale and 1/10-scale), the acceleration scale was selected as approximately 1/5, that is, 5 g on the model equals 1 g on the prototype. This selection was made so that the 1/30-scale model could be tested on the electrodynamic seismic simulator at the Los Alamos National Laboratory and the 1/10-scale model on the servo-hydraulic seismic simulator at the Construction Engineering Research Laboratory (CERL).

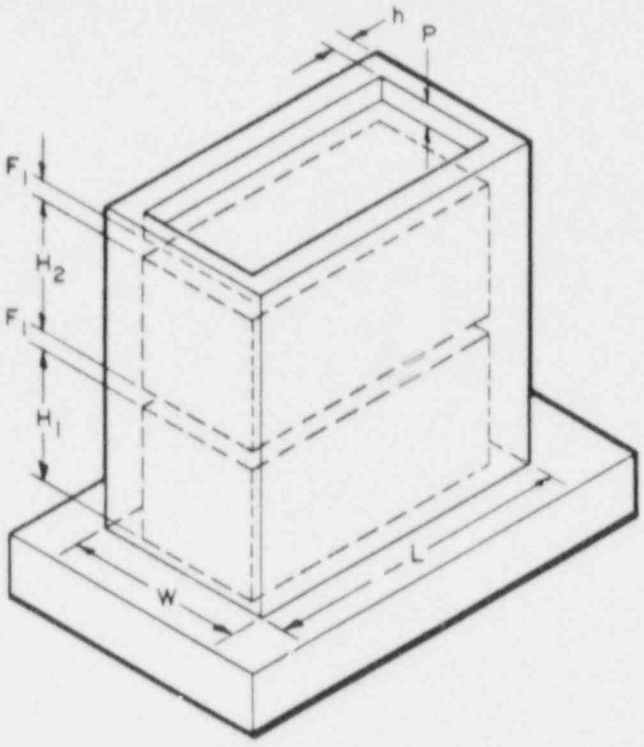

	h, F_1, F_2	W	L	H_1 & H_2	P	Wt/STORY*(lb)
1/30-SCALE	1 in.	10 in.	18 in.	7.25 in.	1 in.	47.7
1/10-SCALE	3 in.	30 in.	54 in.	21.75 in.	3 in.	1286
PROTOTYPE	30 in.	25 ft	45 ft	18 ft, 1.5 in.	30 in.	1,286,000

*BASE NOT INCLUDED

Fig. C-1. Model structure.

For a Case III model, the scaling laws were:

$$N_{\ddot{y}} = Q,$$

$$N_m = \bar{N}_h^2/Q, \text{ and}$$

$$N_t = \sqrt{\bar{N}_h/Q},$$

where $\bar{N}_h$ is the selected length scale and Q is the selected acceleration scale. For a Q value of 1/5, this results in:

for the 1/30-scale structure,

$\bar{N}_h = 30,$

$N_{\dot{y}} = 1/5,$

$N_m = 4500,$ and

$N_t = 12.25.$

For the 1/10-scale structure,

$\bar{N}_h = 10,$

$N_{\dot{y}} = 1/5,$

$N_m = 500,$ and

$N_t = 7.07.$

With the mass scale established, it was possible to design the masses that must be added to the model structures to properly simulate the distributed mass of the prototype. The procedure was as follows:

1. The dynamic lumped mass equivalent of the prototype distributed mass at each level, $(DLME)_p$, was established. (This may involve an energy method calculation, but in many cases, the $(DLME)_p$ is taken as the mass of the structure concentrated at a given level plus a fraction of the distributed mass (walls) on both sides of that level.)
2. The required dynamic lumped mass equivalent of the model distributed mass at each level, $(DLME)_m$, was then computed as

$$(DLME)_m = \frac{(DLME)_p}{N_m} .$$

3. The amount of mass that must be added to the model to obtain the required $(DLME)_m$ was then computed as

$$\text{Required Added Mass} = (DLME)_m - \frac{(DLME)_p}{\bar{N}_h^3}$$

The results of these computations are shown in Table C-I. Note that the fabricated masses were slightly different than the required values. At this point, we had the following two choices:

1. We could have reworked the masses to obtain the desired values.
2. Since these computed values were the result of the selection of Q = 1/5, and since Q need not be exactly this value, we could have used the value of the added masses as fabricated and work backwards to determine the actual scale values that apply. Thus:

a. $$N_{m_{actual}} = \frac{(DLME)_p}{\frac{(DLME)_p}{\bar{N}_h^3} + \text{Actual added mass}} ,$$

b. $$N_{y_{actual}} = Q_{actual} = \frac{\bar{N}_h^2}{N_{m_{actual}}} , \text{ and}$$

c. $$N_{t_{actual}} = \sqrt{\frac{\bar{N}_h}{Q_{actual}}} .$$

The second course was taken, and the actual scales to be used in testing the model and interpreting the results are shown in Table C-I. Note that two different assumptions for the dynamic lumped-mass equivalent of the prototype distributed mass were investigated. As indicated in the body of this report, these two cases gave nearly identical results. The method of attaching the added mass is shown in Fig. C-2.

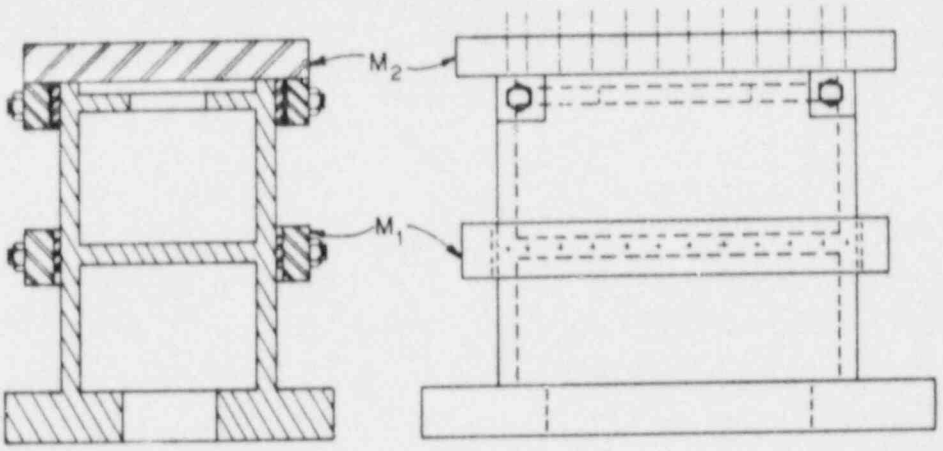

STRUCTURE	SCALE	M_1 (lbs)	M_2 (lbs)
3D-10-2	1/30	228	231
3D-11-2	1/30	228	231
3D-12-2	1/30	236	166
CERL 1	1/10	1285	1330
CERL 2	1/10	1285	906

Fig. C-2. Method of attaching added mass.

With the model construction complete (including the attached masses) and the scales firmly established, the test conditions could be specified. All of the models were to be subjected to a properly scaled version of the 1940 El Centro N-S accelerogram. The base line corrected version of the signal that was selected as the desired prototype base motion input is shown, together with its integrals, in Fig. C-3 (a). At each test facility (Los Alamos and CERL), this signal was entered into the seismic simulator control system in digital form. It was then time-scaled, as appropriate, by changing the assigned time-step value between points. For the tests conducted on structures 3D-10-2 and 3D-11-2 (1/30-scale, N_t = 11.8, tested at Los Alamos), the signal was scaled so that the total test duration was 16/11.8 = 1.36 s, and all frequency components were increased by a factor of 11.8. Likewise, the input signal for the test of 3D-12-2 was time- and frequency-scaled by 12.2; for the test of CERL #1, by 6.8; and for the test of CERL #2, by 7.04.

All of the model structures were subjected to properly time-scaled seismic inputs having a progressively larger peak value, $\ddot{Y}_{pk}$. For structures 3D-10-2

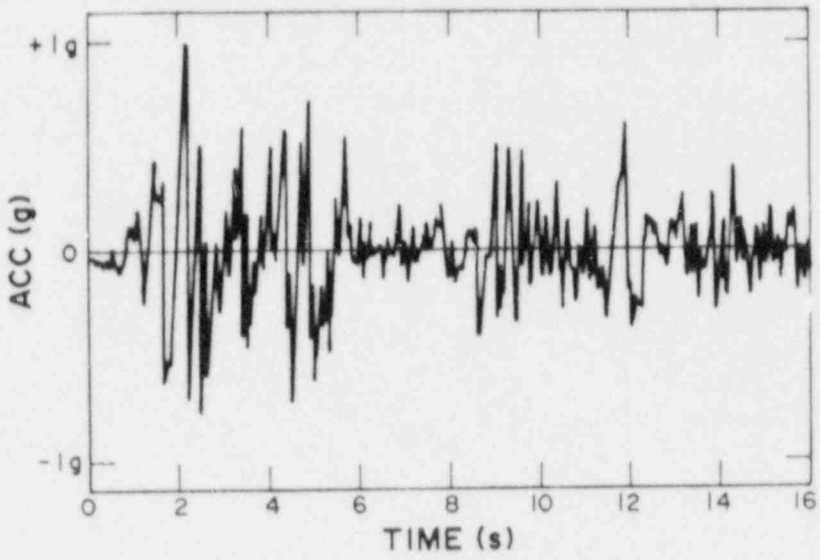

Fig. C-3 (a). 1940 El Centro N-S accelerogram (normalized to 1-g peak).

and 3D-11-2, a peak value of 4.6 g per 1 g of prototype acceleration was used; for 3D-12-2, the ratio was 4.95 g/1 g; for CERL #1, the ratio was 4.6 g/1 g; and for CERL #2, the ratio was 4.95 g/1 g. Measured response accelerations are, of course, interpreted in the same way; i.e. for structurrs 3D-10-2 and 3D-11-2, a 4.6-g response represented 1 g response in the prototype, etc.

Note that velocities ($\dot{y}$) are scaled as $N_{\dot{y}} = N_{\ddot{y}} N_t$ and displacements (y) as $\bar{N}_h$. These scales can be used to check the velocity and displacement limits required of the seismic simulator. As an example, to test structure CERL #1, for which $N_{\ddot{y}} = 1/4.6$ and $N_t = 6.8$,

$$N_{\dot{y}} = 1.48, \text{ and}$$
$$\bar{N}_y = 10.$$

Then (referring to Fig. C-3 (b) and C-3 (c) the peak velocity required per 4.6-g peak acceleration (which simulate 1 g on the prototype) is 37.94/1.48 = 25.66 in./s. The peak displacement required per 4.6-g peak acceleration is 9.82/10 = 0.98 in.

Because the CERL facility has a 30-in./s velocity limit and a $\pm$ 3 in.-displacement limit, we estimate that this model can be tested to the smaller of (30/25.66) x 4.6 = 5.37 g or (3/0.98) x 4.6 = 14.1 g's.

Because this was a short transient signal, the velocity limit was somewhat larger than the value of 30 in./s that was established for steady-state vibration; as a result, the CERL #1 structure was tested to a peak acceleration of over 12 g (with some distortion of the signal frequency content, however).

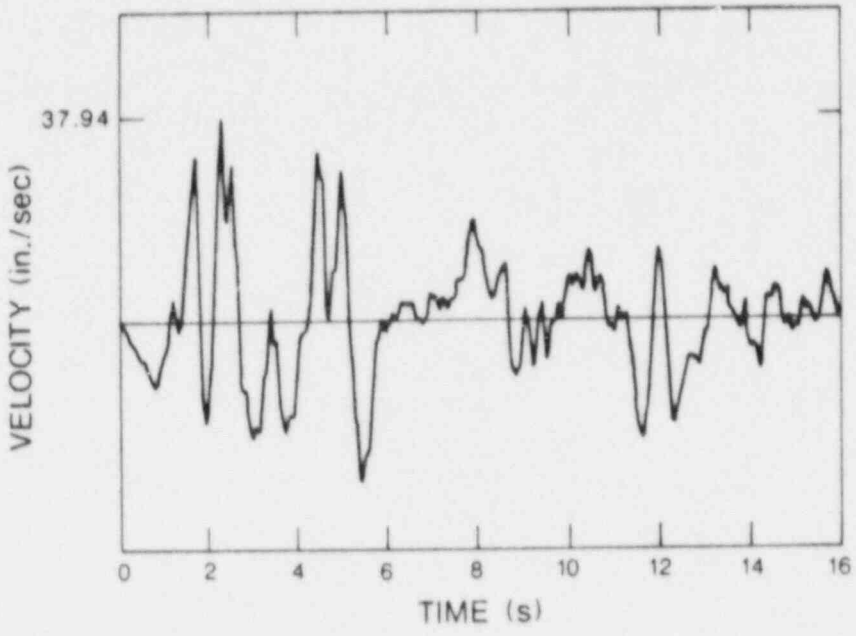

Fig. C-3 (b). 1940 El Centro N-S velocity history (accelerogram normalized to 1-g peak).

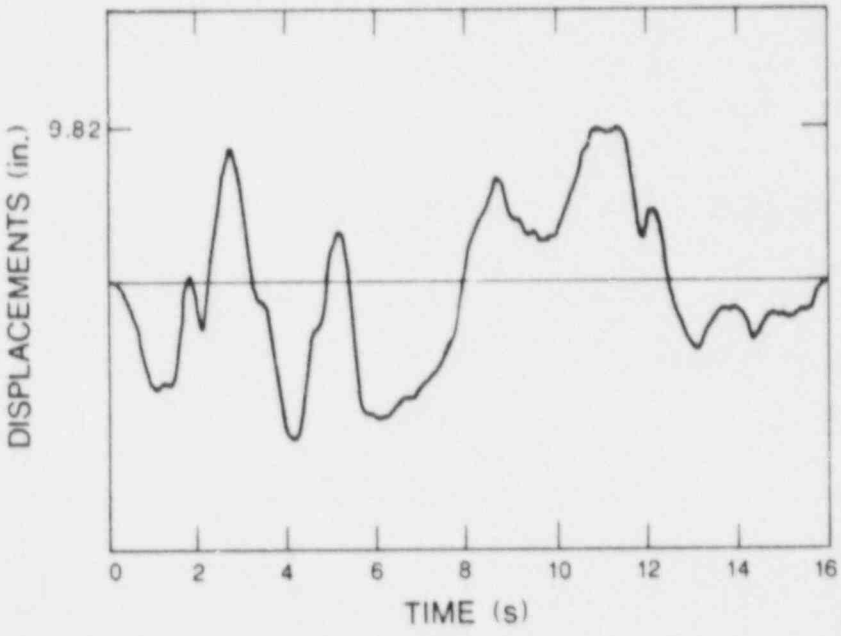

Fig. C-3 (c). 1940 El Centro N-S displacement history (accelerogram normalized to 1-g peak).

TABLE C-I

COMPUTATION OF ADDED MASSES AND SCALES

Model Structure	Assumed $(DLM)_p$ (lb)	Required Added Mass* (lb)	Actual Added Mass** (lb)	Final Scales N_m	$N_{\ddot{y}}$	N_t
1. 3D-10-2 and 3D-11-2 1/30-Scale	1,125,000 at Levels #1 and #2	208 at Levels #1 and #2	228-Level #1 231-Level #2	4172	1/4.6	11.8
2. CERL #1 1/10-Scale	Same as above	1125 at Levels #1 and #2	1285-Level #1 1330-Level #2	462	1/4.6	6.8
3. 3D-12-2 1/30-Scale	1,260,000 at Level #1 888,000 at Level #2	233 at Level #1 164 at Level #2	236 at Level #1 166 at Level #2	4460	1/4.95	12.2
4. CERL #2 1/10-Scale	Same as above	1260 at Level #1 888 at Level #2	1285 at Level #1 906 at Level #2	495	1/4.95	7.04

* For Q = 1/5.

** Includes attachment bolts.

APPENDIX D
FREQUENCY DOMAIN ANALYSIS

I. INTRODUCTION

One of the fundamental relationships calculated in experimental structural dynamics is the transfer function. From this function an analyst may determine experimental values for natural frequencies of a structure and associated damping ratios. In the Seismic Category I Structures Program, all experimental values of natural frequencies and damping ratios are determined from analysis of transfer functions. For the reader who is unfamiliar with transfer functions and the dynamic characteristics of a structure that may be determined from them, this appendix will provide an explanation of these concepts with a minimum of mathematical rigor. In instances where detailed mathematical justifications are left out, either for the sake of brevity or coherence, the reader will be directed to appropriate references for more material.

Since the transfer functions measured in the Seismic Category I Structures Program are all a function of frequency, the discussion will begin by distinguishing between time domain and frequency domain dynamic analysis, with justifications for using frequency domain analysis in experimental applications. Next, the transfer function will be defined and this will be followed by an explanation of how natural frequencies and damping ratios are calculated from a transfer function. Finally, assumptions made in conjunction with the use of transfer functions in dynamic structural analysis along with limitations and sources of error will be discussed.

II. TIME DOMAIN vs FREQUENCY DOMAIN DYNAMIC ANALYSIS

A prerequisite to determining the response of a structure to dynamic loads is the definition of the structure's dynamic properties. The dynamic properties that completely characterize the linear response of a structure are natural frequencies, mode shapes and a measure of damping or equivalent mass distribution, stiffness distribution, and damping. When these properties have been determined, the governing differential equation of motion for the structure can be solved with response being specified either as a function of time

or frequency. If response is specified as a function of time (time is the independent variable), a time domain dynamic analysis is said to have been performed. If response of the structure is specified as a function of frequency (frequency is the independent variable), a frequency domain analysis has been performed.

Experimental dynamic structural analysis is usually concerned with determining the dynamic properties of a structure from measured input and response data. Little information can be determined from a response-time history of a structure if additional experiments are not performed to determine mass and stiffness distributions and, for all but the simplest geometries, the mass and stiffness distributions are difficult to obtain. However, response-frequency spectra (a spectrum is a plot of a variable as a function of frequency) can be used to approximate natural frequencies, mode shapes, and damping without any supplemental experimental measurements. For this reason response-frequency spectra are usually chosen over time domain analysis in experimental applications.

The classical spring-mass-damper system found in most introductory vibrations texts[1] can be used to illustrate an experimental time domain and frequency domain dynamic analysis. In time domain experimental analysis, the mass is excited by a known time-dependent forcing function and the response is measured as a function of time. A separate static load-deflection experiment is needed to determine the spring constant and the mass has to be weighed. Knowing the mass, stiffness, input and response, the damping can then, in theory, be determined by comparing the experimentally measured response to the closed form analytical solution of the differential equation of motion. Once the damping is determined, the spring-mass-damper system's dynamic properties have been defined and the response to a general time-dependent forcing function can be determined analytically. The difficulty in extending this procedure to multi-degree-of-freedom structures becomes evident when one tries to experimentally determine the mass and stiffness distributions of a more complex structure.

In a frequency domain analysis, the spring-mass-damper system is excited by a sinusoidal forcing function and the magnitude of the peak response is plotted as a function of exciting frequency, as the frequency is varied over a specified range. The peak in the response vs frequency plot corresponds to the natural frequency of the system and an estimate of damping can be obtained

from the decay of the peak response. With natural frequency and damping known, the single-degree-of-freedom system's dynamic properties are defined and the equations of motion can be solved for a general forcing function yielding results equivelent to those obtained in the time domain analysis above. This concept can be extended to a multi-degree-of-freedom system, if it is noted that, for each degree of freedom, there will be a corresponding peak in the response spectra and associated damping value. Also, although beyond the scope of this appendix, it should be noted that, with a measured input, the predominent mode shapes corresponding to the measured natural frequencies can be determined without the need for additional experimental measurements.

This section has discussed why we use frequency domain dynamic analysis in experimental structural dynamics. The remainder of the appendix focuses on how frequency domain data are analyzed to determine the dynamic properties of a structure.

III. DEFINING A TRANSFER FUNCTION

The basic relationship that is necessary for experimental determination of a structure's natural frequencies and damping ratios in the frequency domain is the transfer function. If a structure (see Fig. D-1) is excited by a known forcing function, y(t), at some Point A (a base acceleration in the case of Seismic Category I Structures), and if the response, x(t), is measured at some Point B, it is found, in general, that the structure has transformed the input signal to yield the response.

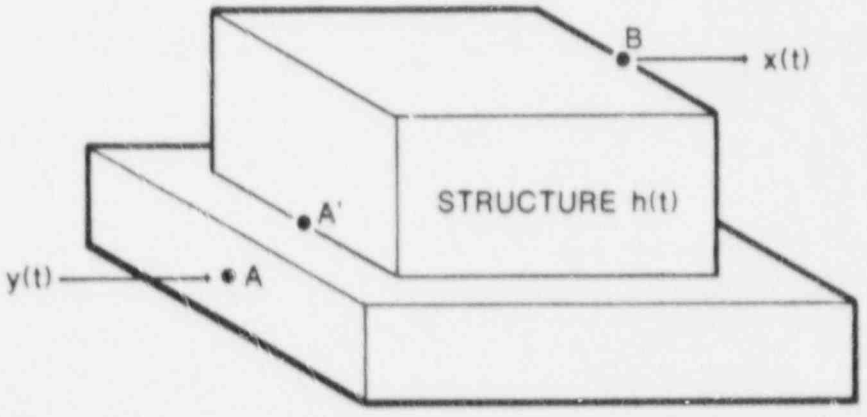

Fig. D-1. Schematic of an instrumented structure.

This transformation is denoted h(t) and the following relationship can be established

$$y_A(t)*h_{AB}(t) = x_B(t) \quad ,$$

where * indicates convolution. This relationship can be transformed into the frequency domain by the Laplace transform as follows:

The Laplace transform of a general time-dependent function, f(t), is

$$F(s) = \int_0^\infty f(t)\, e^{-st} dt \quad , \tag{1}$$

where s is the complex variable of transformation and, in general,

$$s = \sigma + \omega i \quad , \tag{2}$$

and

$$i = \sqrt{-1} \quad , \text{ with}$$

σ = a measure of damping, and

ω = circular frequency.

Applying this to the convolved signals, and noting that convolution in the time domain is equivalent to multiplication in the frequency domain, yields

$$Y_A(s)\, H_{AB}(s) = X_B(s) \quad , \tag{3}$$

where

$$X_A(s) = \int_0^\infty x_A(t)\, e^{-st} dt \quad , \tag{3a}$$

$$Y_B(s) = \int_0^\infty y_B(t)\, e^{-st} dt \text{ , and} \qquad (3b)$$

$$H_{AB}(s) = \int_0^\infty h_{AB}(t)\, e^{-st} dt \text{ .} \qquad (3c)$$

By definition, the Laplace transform of the structure's filtering function is the transfer function relating input at Point A to output at Point B. The transfer function is defined in terms of the Laplace transforms of the input and output signal as follows:

$$H_{AB}(s) = \frac{X(s)}{Y(s)} \text{ .} \qquad (4)$$

Since the transfer function $H_{AB}(s)$, is a function of the complex variable, s, and s is made up of a real and imaginary part, $H_{AB}(s)$ can be thought of as a function of two variables describing a surface over the complex plane. Figure D-2 is a plot of the real and imaginary pait of a transfer function for a single degree-of-freedom system.

It should be emphasized that the transfer function, $H_{AB}(s)$, only relates input and response at two specific points. If the input were moved to another point, say A' in Fig. D-1, an entirely different transfer function would result, and, in general, $H_{A'B}(s)$ $H_{AB}(s)$ for any A' not coincident with A.

The Laplace transform does not lend itself to efficient numerical computation. Therefore, in actual experimental work, a special case of the Laplace transform, the Fourier transform, is used. The Fourier transform of a general time signal, f(t), is:

$$F(\omega) = \int_{-\infty}^\infty f(t)\, e^{-i\omega t} dt \text{ .} \qquad (5)$$

REAL PART OF THE TRANSFER FUNCTION
FOR A SINGLE-DEGREE-OF-FREEDOM SYSTEM

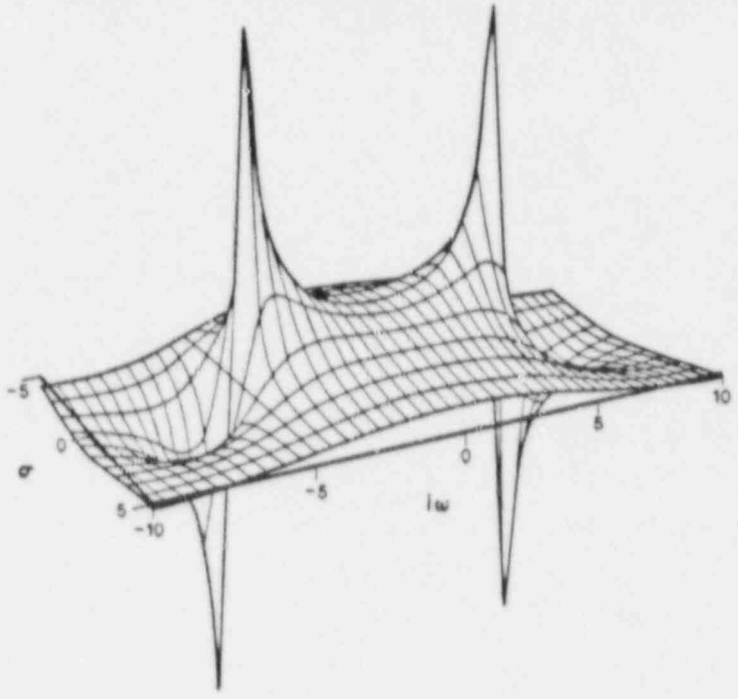

IMAGINARY PART OF THE TRANSFER FUNCTION
FOR A SINGLE-DEGREE-OF-FREEDOM SYSTEM

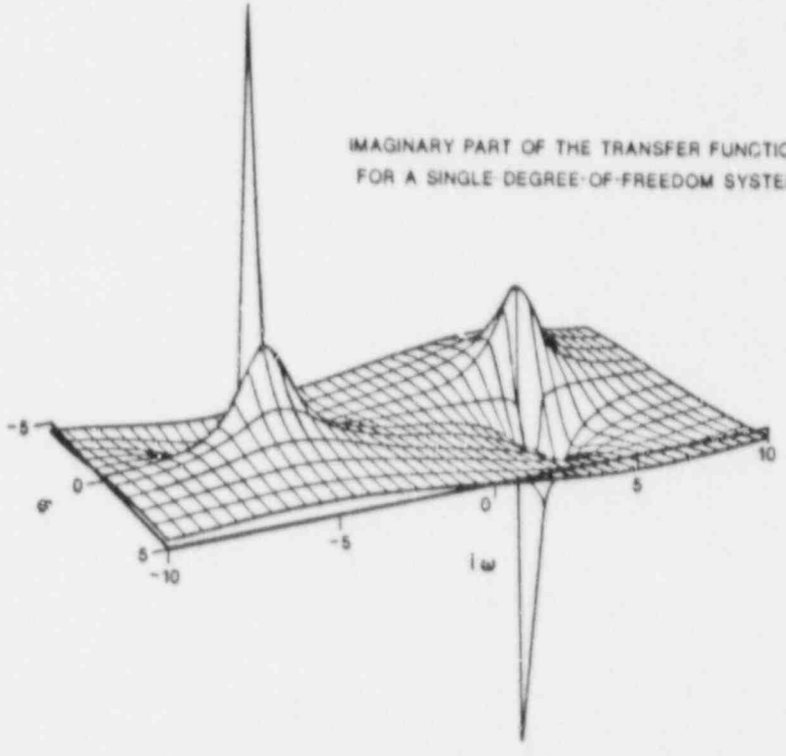

Fig. D-2.

The relationship with the Laplace transform can be easily seen if f(t) is zero for all times t less than zero. The Fourier transform then becomes

$$F(\omega) = \int_0^\infty f(t)\, e^{-i\omega t} dt \quad , \tag{6}$$

and, if the real portion of the Laplace transform is zero ($\sigma = 0$), Eqs. 1 and 6 are equivalent. The Fourier transform, then, is just the imaginary portion of the Laplace transform and can be visualized by passing a plane normal to the complex plane through the $\sigma = 0$ axis, as shown in Fig. D-3. Reference 2 discusses in detail the Laplace transform, the Fourier transform, and the relationship between the two.

The Fourier transform, which is computationally efficient due to the Fast Fourier Transform (FFT) computer algorithm,[3] is employed to calculate a function analogous to the transfer function known as the Frequency Response Function (FRF). The FRF is defined as

$$H_{AB}(\omega) = \frac{X_B(\omega)}{Y_A(\omega)},$$

where

$$Y_A(\omega) = \int_{-\infty}^{\infty} y_A(t)\, e^{-i\omega t} dt \quad , \text{ and}$$

$$X_B(\omega) = \int_{-\infty}^{\infty} x_B(t)\, e^{-i\omega t} dt \quad .$$

A clarification must be made at this point, because the engineering community often uses the term transfer function to mean frequency response function. In a strict sense "transfer function" is the Laplace transform of the function relating input to output and the "frequency response function" is the analogous Fourier transform. However, because the Laplace transform is seldom

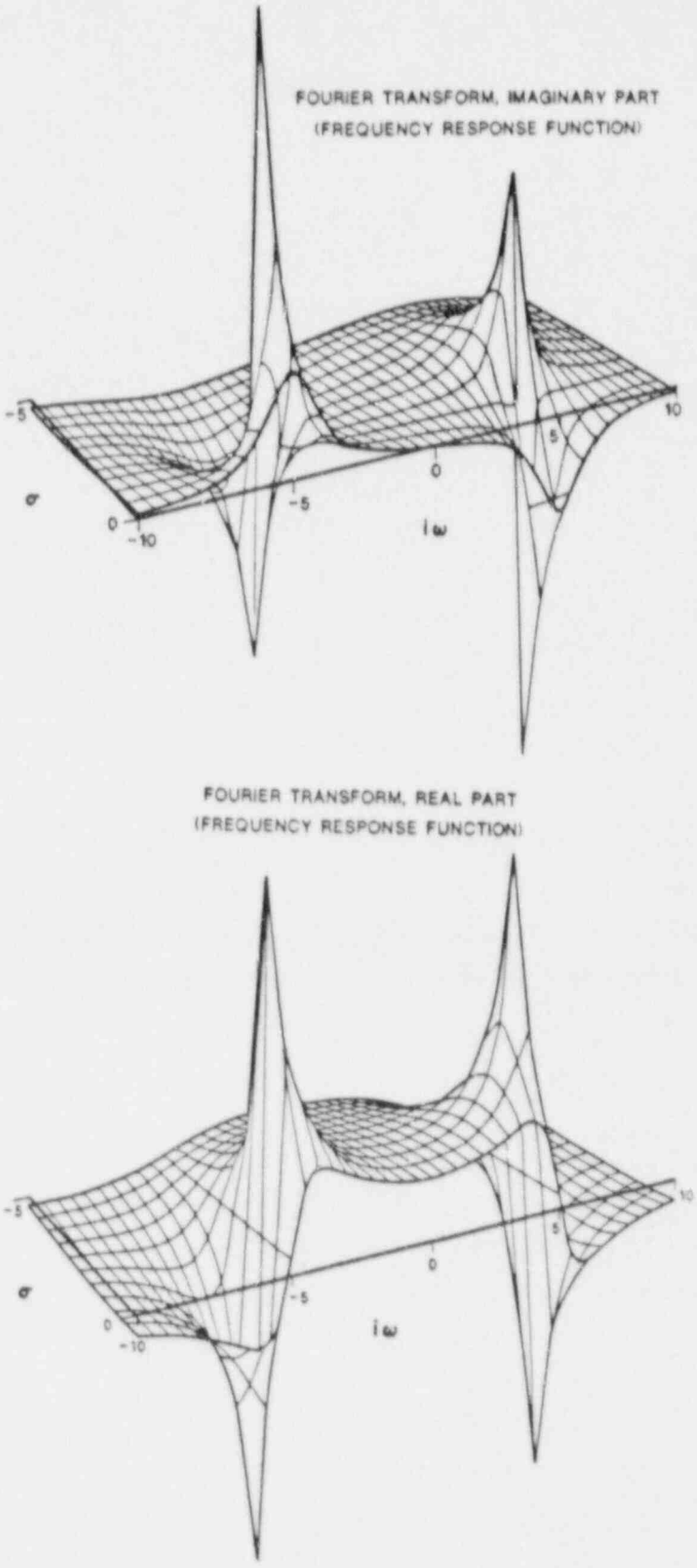
FOURIER TRANSFORM, IMAGINARY PART
(FREQUENCY RESPONSE FUNCTION)
-5
0
-10
σ
-5
0
5
10
iω
FOURIER TRANSFORM, REAL PART
(FREQUENCY RESPONSE FUNCTION)
-5
0
-10
σ
-5
0
5
10
iω

Fig. D-3.

used in actual experimental work, the term "transfer function" has been applied to the frequency response function. The main body of this report is no exception, and, to be consistent with the main body of this report, from this point on "transfer function" will imply Fourier transform and be synonymous with "frequency response function." The term "frequency response function" will not be used any further in this appendix.

In experimental work, the following steps are typical of those required to measure an actual transfer function. First, with current modal analysis hardware, the input and response signals are measured through analog transducers in the time domain. These analog signals are digitized to discrete time domain signals by an analog to digital converter (A to D converter) and then transformed into the frequency domain by means of the FFT algorithm. Both the A to D conversion and the FFT may be accomplished in a single device called a spectrum analyzer. The spectrum analyzer then performs the required calculation relating response to input to determine the transfer function. It should be noted that this process does not produce a continuous function in the frequency domain and, in actuality, the transfer function is a discrete function. Plots of the transfer function look continuous because the discrete points are connected with straight lines.

Response and input may be measured in many ways. Typically, in structural dynamics applications, response is measured as displacement, velocity, or acceleration and input is measured as force, displacement, velocity, or acceleration. Hence, the transfer function can take on many forms depending upon the combination of input and response measurements made. Transfer functions with certain combinations of input and response parameters have been given specific names. The transmissibility function is the transfer function, which relates a displacement response to a displacement input, and mechanical impedance is the transfer function, which relates velocity response to force input. In all testing of the Seismic Category I structural models, the input has been measured as an absolute base acceleration and the output as an absolute acceleration at any point of interest.

The following example will illustrate a closed form calculation of the transfer function for a single-degree-of-freedom base excited structure.

The single-story models tested in this program can be idealized as a single-degree-of-freedom lumped mass system with a base excitation as shown below (Fig. D-4).

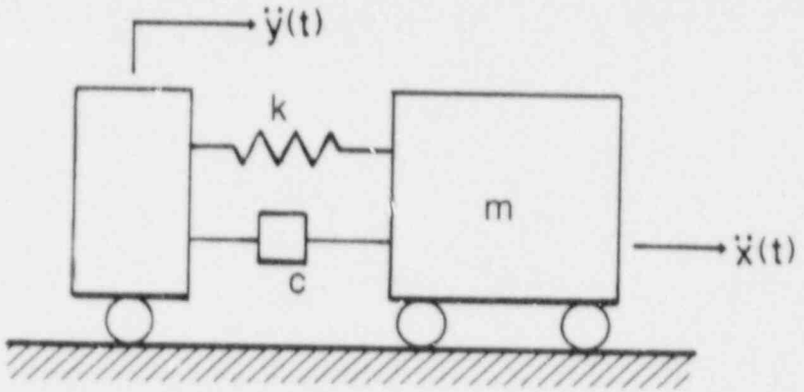

ÿ(t) = SEISMIC BASE EXCITATION
k = STIFFNESS OF THE STRUCTURE'S SHEAR WALL
c = EQUIVALENT VISCOUS CLAMPING OF THE STRUCTURE
m = LUMPED MASS, MASS OF THE TOP-FLOOR SLAB PLUS A PERCENTAGE OF THE WALLS MASS AS DETERMINED BY THE RAYLEIGH METHOD
ẍ(t) = RESPONSE OF THE TOP-FLOOR SLAB

Fig. D-4. Single-degree-of-freedom idealization of a one-story model building.

First, the differential equation of motion must be derived from equilibrium considerations in the time domain. Three forces act on mass m: the inertia force F_m, the spring force F_k, and the damping force F_c, and they all must be in equilibrium.

$$F_m(t) + F_k(t) + F_c(t) = 0 \quad , \tag{7}$$

$$F_m(t) = m\ddot{x}(t) \quad , \text{ where} \tag{7a}$$

$$\ddot{x}(t) = \frac{d^2x(t)}{dt^2} \quad , \text{ and}$$

m is the system mass.

In $F_k(t) = K\,[x(t) - y(t)]$, (7b)

k is the spring stiffness,

$F_c(t) = c\,[\dot{x}(t) - \dot{y}(t)]$, where

$\dot{x}(t) = \frac{dx(t)}{dt}$, $\dot{y}(t) = \frac{dy(t)}{dt}$, and (7c)

c is the damping constant.

Substituting Eqs. 7a-7c into Eq. 7, and separating terms involving base motion, yields the following time domain equation-of-motion for the structure:

$$m\ddot{X}(t) + c\dot{x}(t) + kx(t) = ky(t) + c\dot{y}(t) \quad . \tag{8}$$

Equation 8 will be solved for the transfer function relating the absolute acceleration of the mass to a general time dependent base acceleration excitation. To begin, Eq. 8 is transformed into the frequency domain by means of the Fourier transform as follows:

Let $X(\omega)$ be the Fourier transform of the absolute acceleration response and let $Y(\omega)$ be the Fourier transform of the absolute acceleration base excitation input. Then the Fourier transforms of the displacements and velocities are[5]

$$\int_{-\infty}^{\infty} y(t)\, e^{-i\omega t} dt = \frac{-1}{\omega^2}\, Y(\omega) \quad , \tag{9a}$$

$$\int_{-\infty}^{\infty} \dot{y}(t)\, e^{-i\omega t} dt = \frac{-i}{\omega^2}\, Y(\omega) \quad , \tag{9b}$$

$$\int_{-\infty}^{\infty} x(t)\, e^{-i\omega t} dt = \frac{-1}{\omega^2}\, X(\omega) \quad , \text{ and} \tag{9c}$$

$$\int_{-\infty}^{\infty} \dot{x}(t)\, e^{-i\omega t} dt = \frac{-i}{\omega^2}\, X(\omega) \quad . \tag{9d}$$

Now take the Fourier transform of both sides of Eq. [8]:

$$\int_{\infty}^{\infty} \{m\ddot{x}(t) + c\dot{x}(t) + kx(t)\} e^{-i\omega t} dt = \int_{\infty}^{\infty} \{ky(t) + c\dot{y}(t)\} e^{-i\omega t} dt \quad , \tag{10}$$

and substituting in the above Fourier transforms for velocity and displacement yields the following equation:

$$X(\omega)\left[m - \frac{ic}{\omega} - \frac{k}{\omega^2}\right] = Y(\omega)\left[\frac{-k}{\omega^2} - \frac{ic}{\omega}\right] \quad . \tag{11}$$

The differential equation in the time domain has been transformed into an algebraic equation in the frequency domain. Solving Eq. [11] for $X(\omega)/Y(\omega)$ yields the transfer function relating absolute base acceleration input to absolute acceleration response of the mass in the following manner:

$$H(\omega) = \frac{X(\omega)}{Y(\omega)} = \frac{k + i\omega c}{k + i\omega c - \omega^2 m} \quad , \tag{12}$$

or, in terms of cyclic frequency,

$$H(f) = \frac{1 + i2\zeta f/fn}{1 - (f/fn)^2 + i2\zeta f/fn} \quad , \tag{13}$$

where

$\zeta = \frac{C}{C_c}$, is the damping ratio,

$C_c = 2\sqrt{km}$, is the critical damping value, and

$f_n = \frac{1}{2\pi}\sqrt{\frac{k}{m}}$, is the cyclic natural frequency.

It should be noted that the transfer function was developed for a general base acceleration input and that the transfer function is independent of input.

The transfer function is a complex quantity and can be plotted as either its real and imaginary part vs frequency or its magnitude (also known as gain factor) and phase vs frequency. Figure D-5 is a plot of the closed form analytical solution for the transfer function of a structure with similar mass and stiffness as the single-story 1/30-scale models.

The transfer function may be separated into its real and imaginary parts by rationalizing the denominator in Eq. (13) to obtain

real,

$$\frac{1 - (f/f_n)^2 + (2\zeta f/f_n)^2}{(1 - (f/f_n)^2)^2 + (2\zeta f/f_n)^2} \qquad (14a)$$

imaginary,

$$\frac{-2\zeta(f/f_n)^3}{(1 - (f/f_n)^2)^2 + (2\zeta f/f_n)^2} \qquad (14b)$$

These expressions may be used to determine the magnitude and phase as follows:

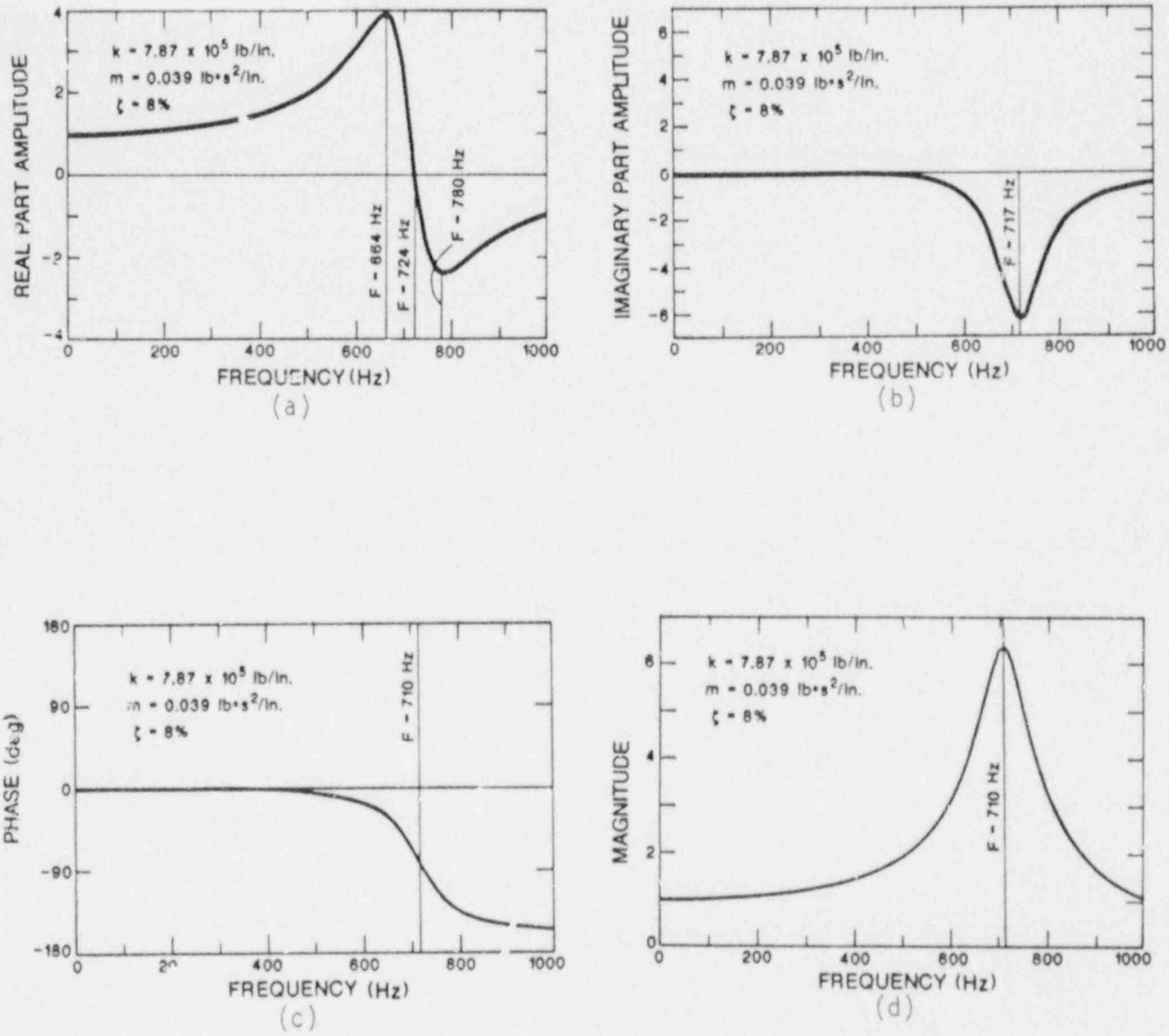

Fig. D-5. (a) S.D.O.F. analytical transfer function calculated with 1/30-scale model properties (real part). (b) S.D.O.F. analytical transfer function calculated with 1/30-scale model properties (imaginary part). (c) S.D.O.F. analytical transfer function calculated with 1/30-scale model properties (phase). (d) S.D.O.F. analytical transfer function calculated with 1/30-scale model properties (magnitude).

$$\text{magnitude} = |H(f)| = \sqrt{(\text{real})^2 + (\text{imag})^2}$$

$$= \left(\frac{1 + (2\zeta f/f_n)^2}{(1 - (f/f_n)^2)^2 + [2\zeta f/f_n]^2} \right)^{1/2} \quad \text{, and} \qquad (15a)$$

$$\text{phase} = \phi(f) = \tan^{-1}\left(\frac{\text{imag}}{\text{real}}\right)$$

$$\tan^{-1}\left[\frac{-2\zeta(f/f_n)^3}{1 - (f/f_n)^2 + 4\zeta^2(f/f_n)^2}\right] . \qquad (15b)$$

To summarize this example, the time domain differential equation-of-motion for the base excited single degree-of-freedom structure was derived based on equilibrium considerations. A general time dependent base acceleration input was specified and the differential equation-of-motion was transformed into a frequency domain algebraic equation. The transfer function was determined from the frequency domain equation and then separated into its real and imaginary parts as well as its magnitude and phase (EOE).

To conclude this section, the concept of a transfer function will be extended to a multi degree-of-freedom base excited structure. The governing set of n differential equations of motion for an n degree of freedom system[5] may be written as follows:

$$[m]\{\ddot{x}(t)\} + [c]\{\dot{x}(t)\} + [k]\{x\} = -[m]\{R\}\,\ddot{y}(t) \quad . \qquad (16)$$

where $[m]$ = n x n mass matrix,

$[c]$ = n x n damping matrix,

$[k]$ = n x n stiffness matrix,

$\{\ddot{x}(t)\}$ = n x 1 vector of absolute accelerations,

$\{\dot{x}(t)\}$ = n x 1 vector of absolute velocities,

$\{x(t)\}$ = n x 1 vector of absolute displacements,

$\{R\}$ — n x 1 vector that associates the base acceleration input, $\ddot{y}(t)$, with the proper degree of freedom on which it acts, and

$\ddot{y}(t)$ = base acceleration input.

The procedure for determining the transfer function is analogous to the single degree-of-freedom case. First, the equation-of-motion is transformed into the frequency domain to obtain

$$\left[[m] - \frac{1}{i\omega}[c] - \frac{1}{\omega^2}[k]\right] \{X(\omega)\} = -Y(\omega)[m]\{R\} \quad . \tag{17}$$

The vector, $\{X(\omega)\}$, is divided by the scalar, $Y(\omega)$, yielding an n x 1 vector, $1/Y(\omega)\ \{X(\omega)\}$, of transfer functions relating the absolute acceleration response at each degree of freedom in the system to the absolute base acceleration input, $X(t)$. If the mass, damping, and stiffness matrices are known, the vector of transfer functions may be solved for analytically as follows:

$$-\frac{1}{Y(\omega)}\{X(\omega)\} = \left[[m] - \frac{1}{i\omega}[c] - \frac{1}{\omega^2}[k]\right]^{-1}[m]\{R\} \quad . \tag{18}$$

IV. DETERMINING NATURAL FREQUENCIES AND DAMPING RATIOS FROM TRANSFER FUNCTIONS

The natural frequency of a lightly damped ($\zeta \leq .1$), single degree-of-freedom (SDOF) system can be determined from the absolute acceleration input--absolute acceleration response transfer function, (see Eq. 13) by noting that the imaginary part of the transfer function (Eq. 14b) reaches a negative peak while the real part, (Eq. 14a) goes to zero, when $f = f_n$ and $h = 0$. With this in mind, the natural frequency of the 1/30-scale model subjected to a seismic base acceleration, as determined from the experimental transfer function plots, Figs. A-6 and B-6, is 64.5 Hz. This technique, that will be referred to as the real and imaginary method (RIM), can be verified by examining the plots of the analytically determined transfer function (Figs. 5A and 5B).

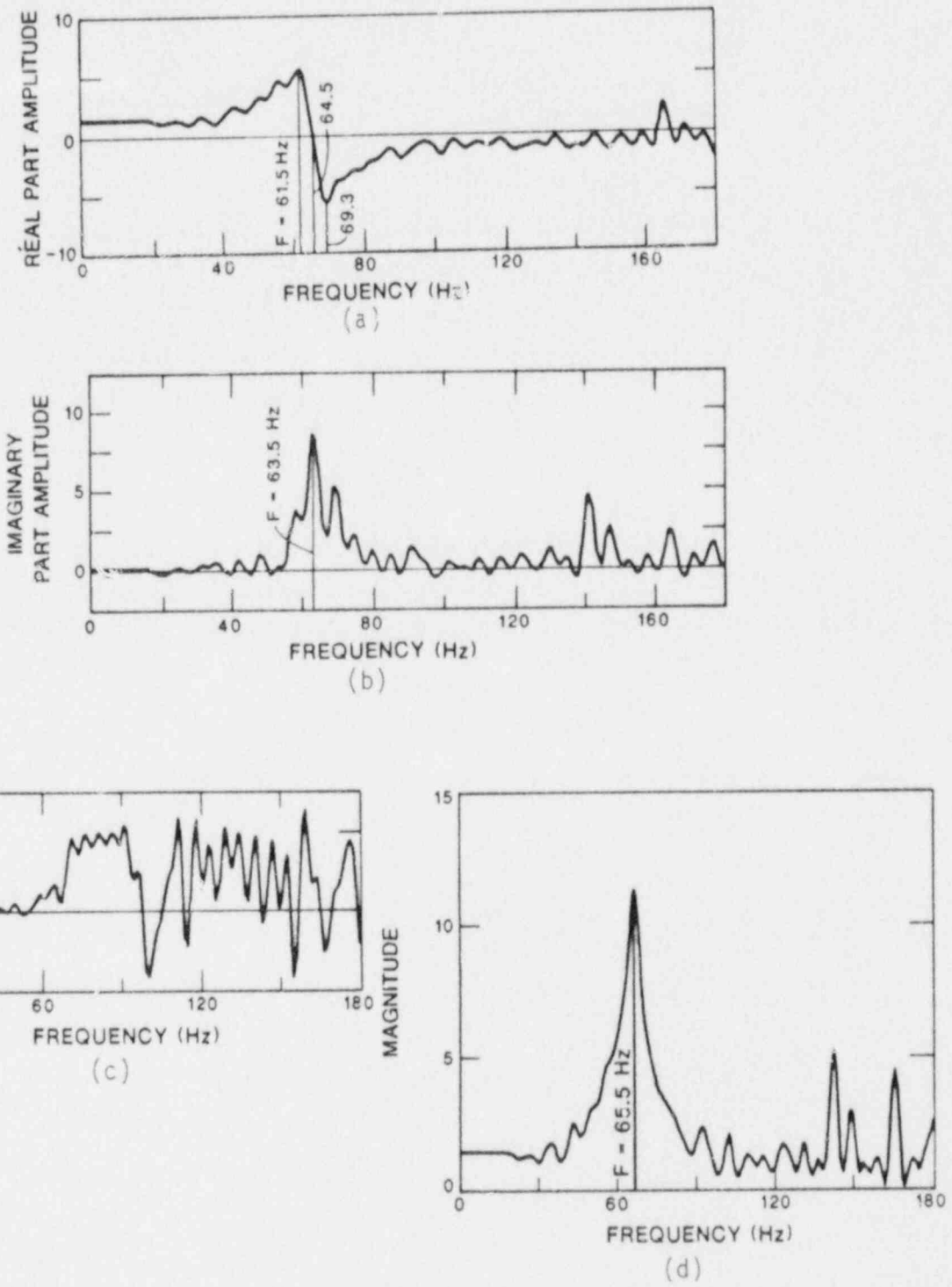

Fig. D-6. (a) Measure transfer function calculated from 1/30-scale model response data (real part). (b) Measure transfer function calculated from 1/30-scale model response data (imaginary part). (c) Measure transfer function calculated from 1/30-scale model response data (phase). (d) Measure transfer function calculated from 1/30-scale model response data (magnitude).

From the parameters used to generate these plots, that natural frequency is known to be

$$f_n = \frac{1}{2\pi}\sqrt{\frac{k}{m}} = 715 \text{ Hz},$$

and the natural frequency of the system as determined from the plots is 717 Hz. This small deviation from the actual natural frequency of the HE system is due to the damping in the system.

Although the algebra is tedious, the mathematical development of the RIM is simply based on finding the roots of Eq. 14a and on finding the points at which Eq. 14b has a zero first derivative and a positive second derivative.

It should be noted that the experimentally determined transfer funcion for the 1/30-scale model has several frequencies at which the real part is zero and the imaginary part has a negative peak. This is due to the fact that this single story model, that has been idealized as a SDOF, short, deep cantilever beam with a concentrated end mass, is, in reality, a continuous structure with many degrees of freedom. The natural frequency with the largest peak corresponds to the shear-bending mode of the SDOF idealization and the other natural frequencies correspond to local modes, such as wall modes.

The RIM may be extended to multi degree-of-freedom (MDOF) systems such as the two- and three-story scale models. These models can be accurately idealized as two- and three-degree-of-freedom systems, respectively. The transfer functions for the two-degree-of-freedom system will have two distinct peaks in the imaginary part, corresponding to two zeroes in the real part; and, similarly, the three-degree-of-freedom system will have three distinct peaks corresponding to zeroes in the real part. In general, if a wide enough frequency range is examined, there will be a natural frequency for each degree-of-freedom in the structure, and, if these natural frequencies are well-separated, they can be accurately determined by examination of the real and imaginary parts of the transfer function. As with the single-story models, the multi-story models will have additional points in their experimental transfer functions that can be identifed as natural frequencies, but these points again pertain to local modes.

The natural frequency of a lightly damped SDOF system may also be determined from the plots of the magnitude and phase of the transfer function. It can be shown that the magnitude reaches a peak while the phase goes through a 180^{o} shift, when $f = f_n$ and $h = 0$. Hence, from Figs. C-6 and D-6, the natural frequency of the 1/30-scale model used previously is 65.5 Hz, as determined from the experimental data. Figures C-5 and D-5 estimate a value of 710 Hz as the natural frequency for the analytical case. This deviation from the actual natural frequency and the fact that the phase change is not a full 180^{o} are both caused by the damping in the system. Note that, for 8% damping, this deviation is less than 1%.

As with the real and imaginary experimental plots, the experimental phase and magnitude plots identify many natural frequencies for the one-story model corresponding to local modes. The extension of the magnitude-phase method of identifying natural frequencies to MDOF systems is analogous to the extension of the RIM to MDOF systems. That is, if the natural frequencies are well-separated and if a wide enough frequency range is examined, there will be a peak in the magnitude corresponding to a 180^{o} phase change for as many natural frequencies as there are degrees-of-freedom.

The damping ratio for a lightly damped SDOF system can be determined from the real part of the transfer function, as shown in Fig. D-7.

Equation 19 may be developed mathematically by taking the real part of the transfer function (Eq. 14a) and by solving for the frequencies where Eq. 14a is a maximum $\left(f_b\right)$ and a minimum $\left(f_a\right)$. Form the ratio f_a/f_b and solve for ζ.

Applying this method to the 1/30-scale model used in the previous example, the real part of the transfer function (Fig. A-6) shows a damping ratio of 5.9%.

This method can be verified by examining the real part of the analytical transfer function plotted in Fig. A-5. From the parameters used to generate this plot, the actual damping ratio is known to be

$$\zeta = \frac{c}{2\sqrt{km}} = 8.0\% \quad ,$$

and the damping ratio as determined from Fig. A-5 is 8.0%.

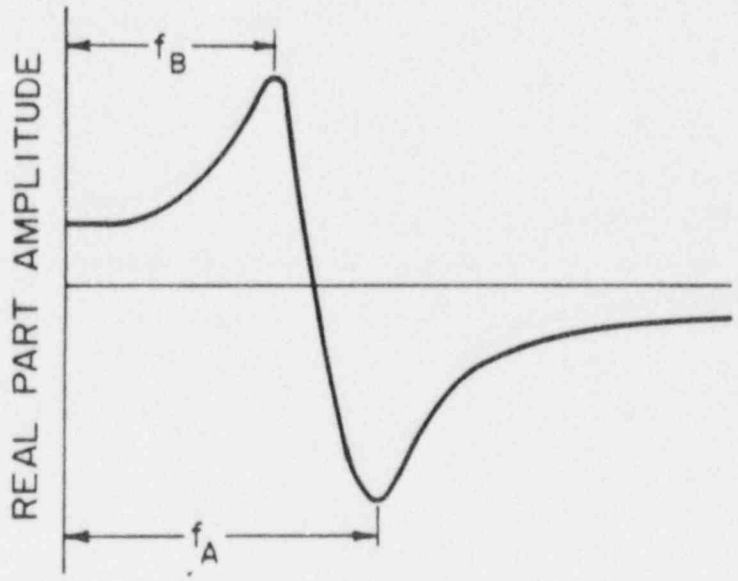

$$Q = \frac{(f_A/f_B)^2 + 1}{(f_A/f_B)^2 - 1}$$

$$\zeta = 1/2Q$$

Fig. D-7. Equivalent viscous damping from transfer function.

This method may be extended to MDOF systems with well-separated natural frequencies by applying the method successively to the peak before and the peak after each natural frequency. This will give the damping ratio associated with that particular natural frequency.

V. ASSUMPTIONS, LIMITATIONS, AND SOURCES OF ERROR

As a final note, the assumptions and limitations of the transfer function techniques for identifying natural frequencies and damping ratios will be discussed and, in some cases, reiterated.

The fundamental assumption for obtaining a transfer function is that the structure's response to a time-dependent-forcing function can be described by a linear second-order differential equation with constant coefficients. All the relationships involving the Fourier and Laplace transforms are based on this assumption, and for low-level excitations, the reinforced-concrete models may be accurately idealized by this type of differential equation. As stated

earlier, the structure is assumed to be lightly damped, that is, to have a damping ratio of less than 10%. This assumption is necessary in establishing the techniques for determining natural frequencies from transfer functions. Damping ratios for the scale models have consistently fallen between 5-8%.

It is also assumed that multi-degree-of-freedom systems have well-separated modes. When the modes are well-separated, the transfer function data can be analyzed as a single degree-of-freedom system in the vicinity of each natural frequency. If the modes are not well-separated, the extension of the single-degree-of-freedom techniques for identifying natural frequencies and damping ratios to multi-degree-of-freedom systems will yield parameter estimates with large error.

The primary sources of error occur in the digitization, the filtering, and on other operations that are performed by the spectrum analyzer. A detailed discussion of these errors is beyond the scope of this appendix and the reader is referred to Ref. 3 for a summary of this topic.

REFERENCES

1. W. T. Thomson, Theory Of Vibration With Application, (Prentice Hall, Inc., New York, 1981), pp. 13-48.

2. C. R. Wylie, Jr., Advanced Engineering Mathematics, (McGraw Hill, Inc., New York, 1966), pp. 221-235.

3. J. S. Bendat, and A. G. Piersol, Random Data: Analysis and Measurement Procedures, (John Wiley and Sons, Inc., New York, 1971), pp. 300-306.

4. R. Bracewell, The Fourier Transform and its Applications, (McGraw-Hill, Inc. New York, 1965), pp. 117-118.

5. R. W. Clough and J. Penzien, Dynamics of Structures, (McGraw-Hill, Inc., New York, 1975), pp 145-150.

APPENDIX E

FLOOR RESPONSE SPECTRA (FRS) MATCHING TECHNIQUE

As pointed out in the body of this report, two methods have been used to determine values for "equivalent viscous damping ratios," from the test data. The "Transfer Functions Analysis Technique," which is discussed in Appendix D, is well-known and widely used. The "Floor Response Spectra (FRS) Matching Technique," which is outlined below, was developed as part of this project effort.

The "FRS Matching Technique" consists of the following steps:

1. A simple, lumped mass analytical model is used in iterative computations.

Because of the way in which the structures used in these tests were constructed and loaded, the two mass models shown in Fig. E-1 with nearly equal masses ($M_1 \sim M_2$), equal stiffness ($K_1 = K_2$), and equal damping ratios ($\zeta_1 = \zeta_2$) are chosen as the appropriate models for the structure in its original condition.

2. Values for M_1 and M_2 are assigned from previous calculations of the effective distributed masses plus the lumped mass added to each story.
3. A value for K_1 and K_2 is assigned to give the analytical model a first-mode frequency equal to the known first mode frequency of the

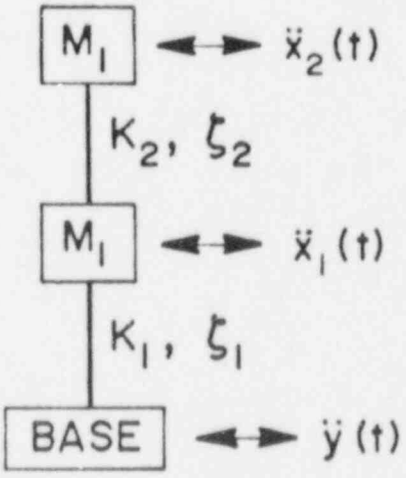

Fig. E-1. Lumped mass model.

structure in its original condition (54 Hz for the CERL No. 1, 1/10-scale structure). A limited amount of trial and error may be involved.

4. A value for ζ_1 and ζ_2 is assigned on a best-guess basis.
5. Using these values, the analytical model is driven with the actual acceleration/time signal to which the structure was subjected during a test. This requires that, for the test chosen, the actual input acceleration/time signal ($\ddot{Y}$ vs t) must be digitized for use in the analytical solution.
6. Response acceleration/time signals ($\ddot{X}_1$ vs t, and $\ddot{X}_2$ vs t) are computed and these signals, in turn, are transformed to FRS, that is, to the procedure outlined in Fig. E-2, (except that the structure "S" is replaced by its analytical model and $\ddot{X}_1$ and $\ddot{X}_2$ are computed rather than measured).
7. The resulting computed FRS plots are compared with the FRS plots previously generated from measured responses and the K and ζ are adjusted until the curves "match."

This procedure has been carried out using the input acceleration/time signal for Test No. 2 on the CERL No. 1, 1/10-scale structure and the mass, stiffness, and damping ratio values are shown on Fig. E-3. The resulting computed

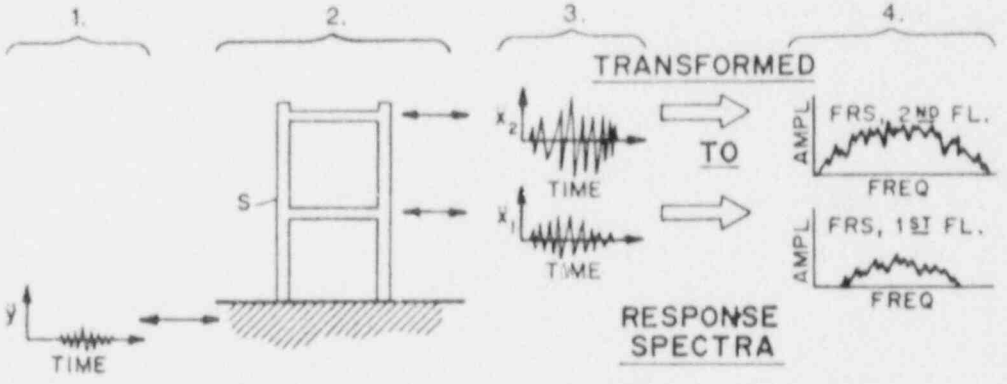

1. $\ddot{y}$ - The input acceleration signal applied to the base of the structure, S.
2. S - A physical structure or an analytical model of the structure.
3. $\ddot{x}_1$ and $\ddot{x}_2$ - The measured (for a physical structure) or computed (for an analytical model) acceleration response at the level indicated.
4. F.R.S. - Floor Response Spectra - The response spectra of the response signal $\ddot{x}_1$ and $\ddot{x}_2$.

Fig. E-2. Computation of floor response spectra, FRS.

FRS are shown on the figure. Comparisons of these computed FRS (Fig. E-3) and the FRS from the measured response during Test No. 2 (Fig. 28) indicate that the analytical model, with the parameter values (M, K, ζ) assigned, is adequate representation of the actual structure at this input level. This "match" was accomplished in five iterations; three trials varying K to adjust f_1 to 54 Hz, and two trials varying ζ to adjust the amplitude of the FRS. Note that the amplitude of the computed second-story FRS does not match the experimentally determined value. Further computation demonstrated that matching both first and second FRS simultaneously could not be achieved using the simple model with $K_1 = K_2$ and $\zeta_1 = \zeta_2$.

This procedure was repeated using the input acceleration/time signals from several additional tests of progressively higher input amplitudes (CERL No. 1, 1/10-scale structure Tests No. 8 and No. 10). In each case, the first-story stiffness (K_1) was adjusted so that the first-mode frequency (f_1) of the analytical model was the same as the measured first mode frequency for that particular test. The value of first damping (ζ_1) was then adjusted as necessary in an attempt to match computed and measured FRS. Values for M_1, M_2, K_2, and ζ_2 were not adjusted; the assumption being that, as the

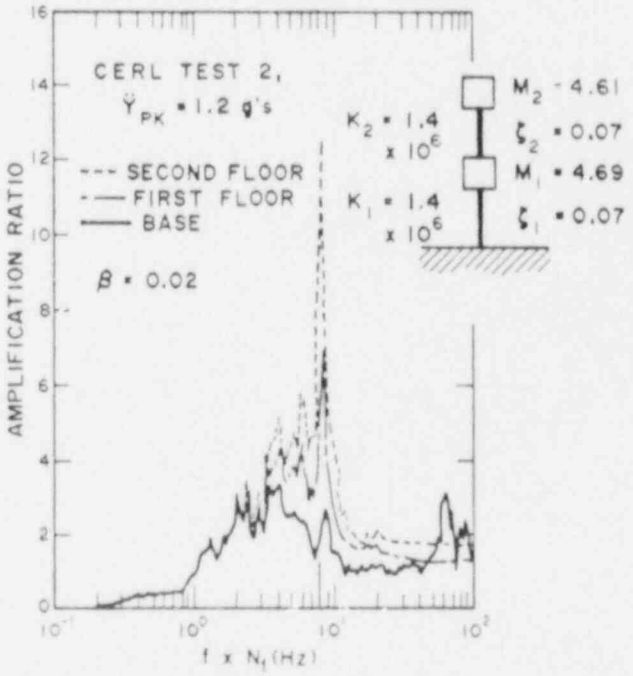

Fig. E-3. Computed FRS, CERL No. 1, $\ddot{Y}_{pk}$ = 1.2 g.

input level increases (at least to some moderate level), only the first-story is undergoing progressive degradation. Figures E-4 and E-5 show the results of these computations. The FRS computed using Test No. 8 input and the analytical model can be compared with those computed from experimental data (Fig. 30.) Clearly the 10% damping ($\zeta_1 = 0.10$) used in the theoretical computation is not large enough to reduce the FRS peak in Fig. E-4 to the peak value determined from experimental data (Fig. 30). This can easily be adjusted by increasing ζ_1; however, we note that the FRS computed from the analytical model do not "match" over the entire frequency range as well as they did for the computation made at lower input level (Test No. 2, Figs. E-3 and 28).

The FRS computed using the analytical model and the input from Test No. 10 (during which failure occurred) are shown in Fig. E-5, and these can be compared with the FRS computed from the measured response, Fig. 31. Here again the first-story FRS peak could be matched by increasing ζ_1; however, the deficiency in the theoretical FRS would still be evident. Specifically, we see that, when only first-story stiffness (K_1) is reduced, at high input levels the model predicts that the first and second stories move together as a rigid body on the first-story walls that are acting as a low-stiffness spring. The experimental data (Fig. 31) shows that this is not the case; hence at high inputs, the assumption that only the first story is damaged is invalid.

Numerous attempts have been made to match thse FRS for the high input level tests by adjusting K_1, and K_2, and ζ_1 and ζ_2. The limited success of these efforts strongly suggests that the linear model (Fig. E-1) is inadequate, even when the parameters have been "tuned." As the required analytical model becomes more complicated, this method for determining damping becomes less appealing.

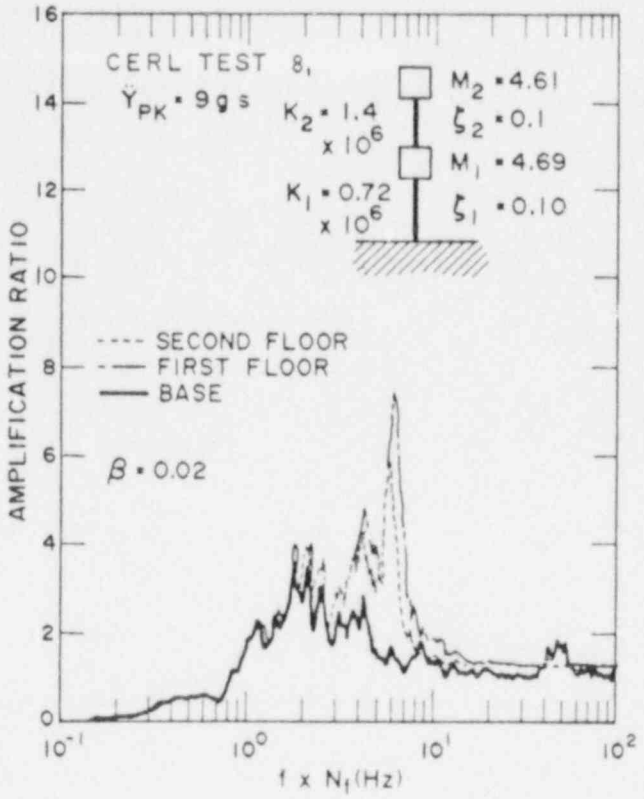

Fig. E-4. Computed FRS, CERL No. 1, $\ddot{Y}_{pk}$ = 9 g.

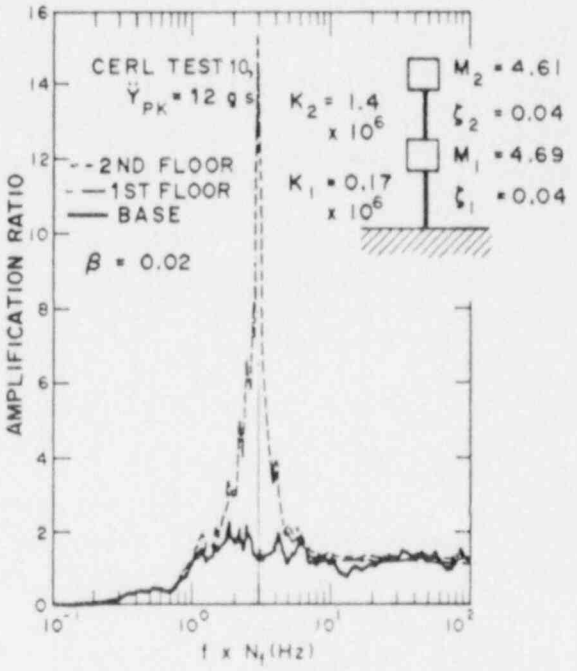

Fig. E-5. Computed FRS, CERL No. 1, $\ddot{Y}_{pk}$ = 12 g.

DISTRIBUTION

	Copies
Nuclear Regulatory Commission, U.S. GPO, Receiving Branch, 8610 Cherry Lane, Laurel, MD 20707	248
Technical Information Center, Oak Ridge, TN 37831	2
Los Alamos National Laboratory, Los Alamos, NM 87545	50
	300

NRC FORM 335 (2-84) NRCM 1102, 3201, 3202

U.S. NUCLEAR REGULATORY COMMISSION

BIBLIOGRAPHIC DATA SHEET

SEE INSTRUCTIONS ON THE REVERSE

1. REPORT NUMBER (Assigned by TIDC, add Vol. No., if any)
NUREG/CR-4924
LA-11013-MS

2. TITLE AND SUBTITLE
Seismic Category I Structures Program
Final Report, FY 1983-84

3. LEAVE BLANK

4. DATE REPORT COMPLETED
MONTH: April YEAR: 1987

5. AUTHOR(S)
Richard C. Dove
Joel G. Bennett
Charles Farrar
Charles A. Anderson

6. DATE REPORT ISSUED
MONTH: September YEAR: 1987

7. PERFORMING ORGANIZATION NAME AND MAILING ADDRESS (Include Zip Code)
Los Alamos National Laboratory
P.O. Box 1663
Los Alamos, NM 87545

8. PROJECT/TASK/WORK UNIT NUMBER

9. FIN OR GRANT NUMBER
A7221

10. SPONSORING ORGANIZATION NAME AND MAILING ADDRESS (Include Zip Code)
Division of Engineering
Office of Nuclear Regulatory Research
US Nuclear Regulatory Commission
Washington, DC 20555

11a. TYPE OF REPORT
Technical

b. PERIOD COVERED (Inclusive dates)
1983-84

12. SUPPLEMENTARY NOTES

13. ABSTRACT (200 words or less)

This report summarizes the results obtained from a series of simulated seismic tests on scale models of a prototypical Category I nuclear power plant auxiliary building, representing a reinforced concrete, diesel generator building. Two sizes of model structures were used: 1/10 scale and 1/30 scale. Model construction, test methods, instrumentation, data reduction techniques, experimental results, comparison of experimental and computed results, and conclusions are presented in this report. Values of structural stiffness obtained from both static and dynamic tests are found to be significantly lower than values of stiffness computed using the usual design methods. Values of modal frequency obtained from dynamic tests are compared with computed values. Decreasing modal frequencies with increasing seismic input are reported. The effective damping of these test structures is determined from the test results. The results obtained from the two different size (1/10- and 1/30-scale) models are compared.

14. DOCUMENT ANALYSIS - a. KEYWORDS/DESCRIPTORS

b. IDENTIFIERS/OPEN-ENDED TERMS

15. AVAILABILITY STATEMENT
Unrestricted

16. SECURITY CLASSIFICATION
(This page) Unc.
(This report) Unc.

17. NUMBER OF PAGES
98

18. PRICE

Available from

Superintendent of Documents
U.S. Government Printing Office
Post Office Box 37082
Washington, D. C. 20013-7982

and

National Technical Information Service
Springfield, VA 22161

Los Alamos